

Exploring the growth mechanism of the electrodeposited carbon components as potential buffer layers for energy storage applications

Apostolopoulou Maria
Department of Electrical and Computer Engineering
Hellenic Mediterranean University

M.Sc. Nanotechnology for Energy Applications

Heraklion, Crete, 2024

Acknowledgements

I would like to express my special thanks to Dr. Dimitra Vernardou for her support, guidance and valuable advice in order to carry out the present work.

I am deeply grateful to Dr. Ricardo Santamaria Ramirez for generously sharing his invaluable expertise and guidance during the preparation of this dissertation.

I would also like to thank all our collaborators in our research laboratory for their help and support.

This dissertation is dedicated to my family and especially to my son, who is a source of inspiration and encouragement that we can always reach our goals.

Abstract

In recent years, the depletion of fossil fuels and environmental pollution has prompted both industry and the scientific community to seek alternative energy sources. Lithium-ion batteries, due to their high energy density, small size, long lifetime and low pollution, have gained a dominant position in everyday life, finding application in portable devices (laptops, smart phones), power tools and electric vehicles. Due to this rapid development of technology, there is growing demand for more efficient energy storage devices. This dissertation aims to investigate carbon-based materials, especially graphene oxide as a potential buffer layer for electrodes in lithium-ion batteries (LIBs) and electrochemical capacitors (ECs). The unique properties of carbon-based materials, such as high surface area, excellent electrical conductivity and tunable pore structures, have led to their widespread application as alternative materials to traditional graphite. The material synthesis procedure was carried out using a graphene oxide dispersion solution, which was prepared by the modified Hummer method. The dispersed solution was the electrolyte in the electrodeposition technique for the immobilization of graphene oxide on copper substrate. The growth mechanism of the material was studied for different deposition time and current. Additionally, the impact of the electrolyte concentration (Li_2SO_4) and the amount of graphene oxide on the electrochemical behavior of the synthesized materials was investigated. Then, the stability of the optimum material obtained (i.e. highest current and material's adhesion) was tested in 600 continuous charge/discharge cycles with sufficiently satisfactory results. In all samples, structural, morphological and electrochemical measurements were carried out by Raman spectroscopy, scanning electron microscopy (SEM), X-ray photoelectron spectroscopy (XPS) and cyclic voltammetry (CV). In conclusion, the dissertation highlights the potential of graphene oxide synthesized via the electrodeposition technique as a cost-effective, rapid, and promising buffer layer for anode materials in energy storage devices.

Keywords: Graphene oxide, Growth mechanism, Buffer layers, Lithium-ion batteries, Electrochemical capacitors.

Table of contents

Acknowledgements **1**
Abstract **2**
Table of contents 3
List of figures 5
List of tables 9
CHAPTER 1. Introduction 10
1.1 Energy Storage Devices and Applications 10
1.2 Capacitors 11
1.3 Lithium ion batteries 11
1.4 Anode materials of Li-ion batteries 13
1.5 Buffer layer 13
1.5.1 Graphene oxide 14
1.5.2 Key requirements for buffer layer 16
1.5.3 Synthesis techniques of graphene oxide 17
1.7 References 20
CHAPTER 2. Synthesis-Experimental part **27**
2.1 Synthesis of graphene oxide 27
2.2 The preparation of graphene oxide dispersion 33
2.3 Substrates 35
2.4 The electrodeposition of graphene oxide buffer layers 35
2.5 Characterisation techniques 37
2.5.1 Raman spectroscopy 37
2.5.2 Scanning electron microscopy/Dispersive X-ray spectroscopy 38
2.5.3 X-Ray photoelectron spectroscopy 40
2.5.4 Cyclic voltammetry 41
2.6 References 43
CHAPTER 3. The effect of deposition time on the synthesis **45**
of graphene oxide 45
3.1 Introduction 45
3.2 Raman Spectroscopy Results 45
3.3 SEM Results 47
3.4 XPS Results 49
3.5 Electrochemical Results 51
3.5 References 57
CHAPTER 4-The effect of electrolyte concentration on the electrochemical performance of graphene oxide **60**
4.1 Electrochemical Results 60
4.2 Stability of the GO in different electrolyte concentrations 64
4.2.1 Electrochemical Results 64
4.2.2 SEM/EDS Results 65
4.2.3 XPS Results 68
4.3 References 71
CHAPTER 5. Effect of graphene oxide ratio on the electrochemical performance of graphene

oxide....72
5.1 SEM Results....72
5.2 Electrochemical Results....73
CHAPTER 6. Effect of deposition current density on the electrochemical performance of graphene oxide....76
6.1 Raman Spectroscopy Results....76
6.2 SEM Results....78
6.3 Electrochemical Results....80
6.4 References....83
CHAPTER 7. Conclusions....84

List of figures

Figure 1.1 The graphene oxide molecular structure consists of carbon, hydrogen and oxygen.
Figure 2.1. Oxidation of graphite by $NaNO_3$ and H_2SO_4.
Figure 2.2. Color change of the solution to green after the addition of $KMnO_4$.
Figure 2.3 Color change of the solution to brown after the addition of 80 ml DIH_2O.
Figure 2.4 Color change of the solution to yellow after the addition of 200 ml DIH_2O.
Figure 2.5 Solution after the addition of DIH_2O to remove impurities.
Figure 2.6. The GO flakes.
Figure 2.7 The GO powder.
Figure 2.8 The homogenization of the GO solution.
Figure 2.9 The GO dispersion through the ultrasonic probe.
Figure 2.10 The metrohm autolab potentiostat/galvanostat system.
Figure 2.11 The three-electrode electrochemical cell consisted of the Ag/AgCl (blue) as reference, the graphite as counter (black) and the Cu substrate as working electrode (red) along with the dispersed GO solution as electrolyte.
Figure 2.12 The three-electrode electrochemical cell consisted of the reference Ag/AgCl(blue), the counter graphite (black) and the working electrode being the synthesized sample on Cu (red) with Li_2SO_4 acting as electrolyte.
Figure 3.1 Raman spectra of synthesized samples with a constant deposition current density of 0.25 mA/cm^2 at different deposition times of 3 minutes (black line), 5 minutes (red line) and 10 minutes (blue line).
Figure 3.2 The diagram of the I_D/I_G ratio as a function with the different deposition times.
Figure 3.3 SEM images of a) 3 min, b) 5 min, c) 10 min deposition time of GO on Cu substrate with 0.25 mA/cm^2 deposition current density. The magnification in all images is x 1500 and the line is equal to 10 μm.
Figure 3.4 The cross-section SEM analysis of the samples a) 3 min, b) 5 min, c) 10 min deposition time with 0.25mA/cm^2 deposition current density. The magnification is x15,000 and the line is equal to 500 nm.
Figure 3.5 C1s XPS spectra of the sample for 3 min deposition time with 0.25 mA/cm^2 deposition current density.
Figure 3.6 O1s XPS spectra of the sample for 3 min deposition time with 0.25 mA/cm^2 deposition current density.

Figure 3.7 Specific Current-Potential curves of the samples for 3 min (black line), 5 min (red line), 10min (blue line) deposition time with 0.25mA/cm^2 deposition current density.
Figure 3.8 Specific Current-Potential curves of 3 min deposition time sample at different scan rates ranging from 5 to 50 mV/s.
Figure 3.9 Cyclic voltammograms of 5 min deposition time sample at different scan rates ranging from 5 to 50 mV/s.
Figure 3.10 Cyclic voltammograms of 10 min deposition time sample at different scan rates ranging from 5 to 50 mV/s.
Figure 3.11 Diffusion Coefficient of the electrodeposited GO for 3 min.
Figure 4.1 Specific Current-Potential curves of the samples for 0.1 M (black line), 1 M (red line) and 0.5 M Li_2SO_4 (blue line) as inset with 3 min deposition time for 0.25mA/cm^2 deposition current density.
Figure 4.2 Specific Current-Potential graphs of 3-min GO electrodeposited sample in 0.1 M Li_2SO_4 at different scan rates.
Figure 4.3 Specific Current-Potential graphs of 3-min GO electrodeposited sample in 1 M Li_2SO_4 at different scan rates.
Figure 4.4 Specific Current-Potential graphs of 3-min GO electrodeposited sample in 0.5 M Li_2SO_4 at different scan rates.
Figure 4.5 Diffusion coefficient of electrodeposited GO samples studied in 0.1 M (black line), 0.5 M (red line), 1 M Li_2SO_4 (blue line).
Figure 4.6 Specific Current-Potential graphs of electrodeposited GO samples studied in 0.1 M Li_2SO_4 for 1, 250, 500 and 600 scans.
Figure 4.7 Specific Current-Potential graphs of electrodeposited GO samples studied in 1 M Li_2SO_4 for 1, 250, 500 and 600 scans.
Figure 4.8 Elemental mapping and EDS of the electrodeposited GO studied in 0.1M Li_2SO_4 electrolyte before CV
Figure 4.9 Elemental mapping and EDS of the electrodeposited GO studied in 1 M Li_2SO_4 electrolyte after CV
Figure 4.10 Elemental mapping and EDS of the electrodeposited GO studied in 0.1M Li_2SO_4 electrolyte after CV
Figure 4.11 SEM images of the electrodeposited GO studied in 0.1M Li_2SO_4 electrolyte after CV

Figure 4.12 SEM images of the electrodeposited GO studied in 1M Li_2SO_4 electrolyte after CV
Figure 4.13 C1s XPS spectra after CV of the electrodeposited GO sample studied in a) 0.1 M $Li_2SO_4$and b) 1 M Li_2SO_4.
Figure 4.14 O1s spectra after CV of the electrodeposited GO samples studied in a) 0.1 M Li_2SO_4 and b) 1 M Li_2SO_4
Figure 5.1 SEM images of a) 2:1 GO:H_2O ratio and b) 3:1 GO:H_2O ratio at 3 min deposition time with 0.25 mA/cm^2 deposition current density.
Figure 5.2 SEM images of a) 2:1 GO:H_2O ratio b) 3:1 GO:H_2O ratio at 3 min deposition time with 0.25 mA/cm^2 deposition current density.
Figure 5.3 Specific Current-Potential graphs of samples 2:1 GO:H_2O and 3:1 GO:H_2O ratio studied in 0.1 M of Li_2SO_4 electrolyte.
Figure 5.4 Specific Current-Potential curves of 3:1 GO:H_2O ratio sample studied in 0.1 M of Li_2SO_4 electrolyte at different scan rates ranging from 5 to 50 mV/s
Figure 6.1 Raman spectra of synthesized samples with a constant deposition time 5 min and deposition current densities, 0.25 mA/cm^2 (black line), 0.5 mA/cm^2 (red line) and 0.75 mA/cm^2 (blue line).
Figure 6.2 The diagram of the ID/IG ratio as a function with the different deposition current densities.
Figure 6.3 SEM images of GO samples with a) 0.25 mA/cm^2, b) 0.5 mA/cm^2 and c) 0.75 mA/cm^2 deposition current densities on Cu substrate with 5 min deposition time. The magnification in all images is x 7,500 and the line is equal to 2 μm.
Figure 6.4 The cross-section SEM analysis of a) 0.25 mA/cm^2 b) 0.5 mA/cm^2 and c) 0.75 mA/cm^2 deposition current density for 5 min deposition time. The magnification in a,b and c images is x 50,000 and the line is equal to 500 nm.
Figure 6.5 Specific Current-Potential curves of the GO electrodeposited samples with 0.25 mA/cm^2 (red line) 0.5 mA/cm^2 (black line), 0.75 mA/cm^2 (blue line) deposition current density for 5 min deposition time.
Figure 6.6 Specific Current-Potential curves of electrodeposited GO for 0.25mA/cm2 at different scan rates ranging from 5 to 50 mV/s.
Figure 6.7 Specific Current-Potential curves of electrodeposited GO for 0.5 mA/cm^2 at different scan rates ranging from 5 to 50 mV/s.

Figure 6.8 Specific Current-Potential curves of electrodeposited GO for 0.75 mA/cm^2 at different scan rates ranging from 5 to 50 mV/s.

List of tables

Table 2.1. Precursor materials for the three main steps of graphene oxide synthesis - oxidation, exfoliation and purification.
Table 2.2 The series of samples performed and the parameters (bold) changed in each series including deposition time, electrolyte concentration, GO:H_2O ratio and deposition current.
Table 3.1 The thicknesses of electrodeposited GO for deposition time 3 min,5 min and 10 min with 0.25 mA/cm^2 current density.
Table 4.1 The at. % of elements before and after CV of the electrodeposited GO studied in 0,1 and 1 M Li_2SO_4 electrolyte.
Table 6.1. The thicknesses of electrodeposited GO for 5 minutes with 0.25 mA/cm^2 0.5 mA/cm^2 and 0.75 mA/cm^2 current density.

CHAPTER 1. Introduction

1.1 Energy Storage Devices and Applications

Energy storage devices are used to accumulate energy in particular equipment or systems so that it can be used at a later time as needed [1,2]. There are several types of energy storage devices, including batteries, thermal, mechanical, pumped hydro, and hydrogen [1,2]. Batteries are the oldest, most common, and widely accessible form of storage encompassing a range of systems. For instance, thermal systems use heating and cooling methods to store and release energy, while mechanical systems draw on the kinetic forces of rotation or gravitation to store energy. Pumped hydroelectric facilities are the most common form of energy storage on the grid and account for over 95% of the storage in use today. On the other hand, hydrogen energy storage is still emerging and involves its conversion from electricity via electrolysis for storage in tanks. There are several types of energy storage systems [3,4,5], including:

1. Batteries: These include lithium-ion, nickel-metal hydride, and lead-acid batteries, among others. They are commonly used for energy arbitrage, backup power, demand charge reduction, and voltage support.
2. Thermal Storage: This involves storing energy in the form of heat or cold in a solid, liquid, or air. Examples include molten salt storage and ice-based storage systems.
3. Mechanical Storage: This includes flywheels, pumped hydro storage, gravity energy storage, compressed air energy storage, and rail-based advanced energy storage.
4. Electrochemical Storage: This includes various battery technologies that use different electrochemical reactions, such as lithium-ion batteries, sodium-sulfur batteries, and flow batteries.
5. Hydrogen Storage: This is an emerging technology that involves converting electricity via electrolysis for storage in tanks. From there, it can be re-electrified or used for emerging applications such as transport, industry, or residential use.

These are just a few examples of the many types of energy storage systems available. The appropriate system depends on the specific application and must consider factors such as the charge and discharge profiles, storage capacity capability, scale of the system, and response time needed.

1.2 Capacitors

Capacitors consist of two conductors separated by a nonconductive material known as a dielectric. They store electric charges through electrostatic attraction between opposite charges accumulated at the plates. Structural capacitors can be integrated into multifunctional materials, providing both mechanical support and electrical energy storage capabilities [6].

Capacitors excel in delivering rapid bursts of current due to their ability to release stored energy quickly. They find application in various fields such as pulse power supplies, filtering circuits, and energy recovery systems. However, they have relatively lower energy densities compared to batteries [7].

An emerging technology is the lithium-ion capacitor (LIC), which combines the benefits of both capacitors and lithium-ion batteries. These devices offer higher energy density than traditional capacitors, while maintaining fast charging and discharging rates. Recent studies focus on optimizing active materials, modeling thermal management systems, and improving cycle life predictions [8].

In contrast to batteries, capacitors do not involve chemical reactions or redox processes during operation. Instead, they rely solely on electrostatic interactions. As a result, capacitors exhibit significantly faster response times and longer life spans without any capacity fade. On the other hand, batteries deliver higher energy densities and more extended runtime per charge cycle [9].

Research efforts continue to explore novel materials and designs for improved performance in both capacitors and batteries. For instance, structural supercapacitors show promise in integrating advanced functionalities within existing infrastructure, making them attractive candidates for next-generation energy storage solutions [6,7].

1.3 Lithium ion batteries

Lithium-ion batteries (LIBs) consist of a cathode, an anode, and a separator soaked in an electrolyte. The cathode typically contains lithium-metal oxides like LiCoO2, while the anode often consists of lithium-carbon compounds. During operation, lithium ions move from the anode to the cathode through the electrolyte, while electrons flow from the anode to the cathode through the external circuit. This movement of ions and electrons generates electrical energy [10,11,12].

The electrochemistry of LIBs involves oxidation-reduction (redox) reactions. Reduction occurs at the cathode, where cobalt oxide combines with lithium ions to form lithium-cobalt

oxide ($LiCoO_2$) [13] On the other hand, oxidation takes place at the anode, where graphite intercalation compounds form graphite and lithium ions. These reactions determine the capacity and voltage of the battery [14,15].

LIBs are crucial for powering portable electronics and are promising for electrifying the transport sector due to their high energy density. They are widely used in mobile devices, electric vehicles, and various electronic gadgets due to their high charge density and rechargeable nature.

Non-aqueous LIBs typically use lithium-metal oxides as cathodes and graphite as anodes with a liquid electrolyte containing lithium salts. They offer higher cell voltages (around 3-4 V) compared to aqueous systems (1-2 V), providing more energy density. Aqueous systems have lower voltages, but may offer advantages in terms of safety and cost [14,15]. They are emerging as a promising alternative to traditional lithium-ion batteries due to their advantages such as low cost, safety, high ionic conductivity, and environmental friendliness. These batteries use water-based electrolytes instead of organic electrolytes, offering improved safety and reduced risk of thermal runaway. Research on various aqueous battery systems utilizing lithium, zinc, sodium, magnesium, and aluminum ions as carrier ions is ongoing [16]. The development of suitable electrode materials remains a challenge for these systems. Aqueous batteries have potential applications in electric vehicles, energy storage systems, and other fields requiring energy storage solutions.

Recent research and review articles highlight the challenges and possibilities for aqueous battery systems [16]. A comparison between aqueous and organic electrolytes for lithium-ion batteries shows advancements in different types of electrolytes in terms of the evolution of efficient and safe energy storage solutions. [17]. Studies have also demonstrated the feasibility of lithium-ion batteries using aqueous electrolyte solutions, showcasing stable working voltages and improved safety features [18]. Key materials (i.e. cathode, anode and electrolyte) for aqueous rechargeable lithium-ion batteries have been reviewed to enhance their performance [19].

These advancements in aqueous electrolyte lithium-ion batteries offer a promising avenue for developing safer, more cost-effective, and environmentally friendly energy storage solutions with high ionic conductivity.

1.4 Anode materials of Li-ion batteries

The anode is an important part of a lithium-ion battery and, depending on its properties and morphology, has a strong influence on the overall performance of the whole battery. Due to its structure, graphite as well as carbon-based materials are mainly used as anode materials. Lithium ions can be easily inserted into the large gaps between the carbon atoms, thus preventing the change in the structure of the anode material during the discharging process [14].

The most promising carbon-based electrode materials for energy storage applications include:

1. Graphene: Graphene has emerged as a promising electrode material for energy storage devices due to its exceptional electrical conductivity and large specific surface area [57].
2. Carbon Nanotubes (CNTs): CNTs exhibit excellent electron transport, high electrical conductivity, and accessibility to electrolytes, making them potential materials for the production of electrodes [58].
3. Activated Carbon (AC): Activated carbon is widely used as an electrode material in supercapacitors due to its high surface area, good electrical conductivity, and chemical stability, which make it suitable for high-energy and high-power energy storage devices [59].
4. Carbon Fibers: Carbon fibers have attracted significant research attention as potential electrode materials for energy storage due to their extraordinary properties, such as high conductivity and mechanical strength [60].

These carbon-based materials offer high performance and are being extensively researched for their in application various energy storage devices, including capacitors and batteries.

1.5 Buffer layer

In LIBs, incorporating a buffer layer at the current collector-electrode interface serves multiple purposes, enhancing overall battery performance and longevity. The buffer layer acts as a mediator, promoting uniform lithium-ion transport across the interface and mitigating side reactions that could otherwise compromise battery integrity [20]. Carbon, particularly amorphous carbon, is a widely recognized buffer layer material due to its ability to facilitate lithium-ion transfer and provide excellent electrochemical stability [21,22].

Research indicates that buffer layers like $Li_{0.33}La_{0.55}TiO_3$ Li, Li_3PO_4-Li_3BO_3 composites, significantly enhance the cycling performance and rate capabilities of LIBs. These buffer layers stabilize the electrochemical potential at the interface, preventing rapid degradation

caused by side reactions and maintaining optimal conditions for lithium-ion mobility [21,22,23].

Carbon-based layers are commonly used as buffers in lithium-ion batteries to improve their performance. Some of the most well-known carbon-based layers include carbon nanotube buffer layers, double-buffer silicon-carbon anode materials, and hierarchical buffer structures for silicon/carbon composites [24,25,26]. These buffer layers are important because they can help to improve the stability and cycling performance of the battery, as well as prevent the degradation of the electrode materials over time. For example, carbon nanotube buffer layers have shown to reduce the charge transfer resistance and increase the Li ion diffusion coefficient in lithium-ion batteries [24]. Similarly, double-buffer silicon-carbon anode materials have been found to improve the capacity retention and cycling stability of the battery [25]. Overall, the use of carbon-based buffer layers is an important strategy for improving the performance and longevity of lithium-ion batteries.

1.5.1 Graphene oxide

Graphene oxide is a carbon-based material with hydroxyl, epoxy, carboxyl, and other functional groups attached to its basal planes and edges. It is usually produced by the Hummers method, which involves the oxidation of graphite. It has a layered structure with oxygen-containing functional groups on its surface (Figure 1.1). It can be functionalized by non-covalent and covalent approaches, which can enhance its mechanical, electrical, and chemical properties. Graphene oxide has potential applications in various fields, including energy storage, catalysis, sensors, and biomedical research. It can be employed in catalysis for converting polluting gasses during industrial processing. It has high conductivity, which makes it useful in electronic devices. The synthesis of graphene oxide remains a complex procedure, and its isolation is challenging [27,28,29]. The future of surface functionalization of graphene oxide is promising, and researchers are exploring new methods to enhance its mechanical, electrical and chemical properties. For example, Hu et al. investigated silanization combined with reduction and in situ co-polymerization as methods to functionalize the hydroxyl groups of GO in order to improve tensile strength and solubility [61]. In 2018, a study reported that p-p stacking and electrostatic interactions enhance the electrical properties of GO, improving the electron transfer process, increasing the specific capacitance and reducing the internal resistance. Wang et al. investigated the functionalization of thermally reduced GO (trGO) with pyrene derivatives terminated by the hydrogen bonding unit ureidopyrimidinone (UP) to form (trGO)-UPPY.68 The graphene

surface was modified with pyrene groups which formed π-π bonds with UPPY. This Layer-by-Layer (LBL) self-assembly technique was repeated to form trGO-UPPY films composed of both hydrogen bonds and π-π bonds. The resulting multilayered films demonstrated potential as excellent electron conductors to improve electron transport [62].

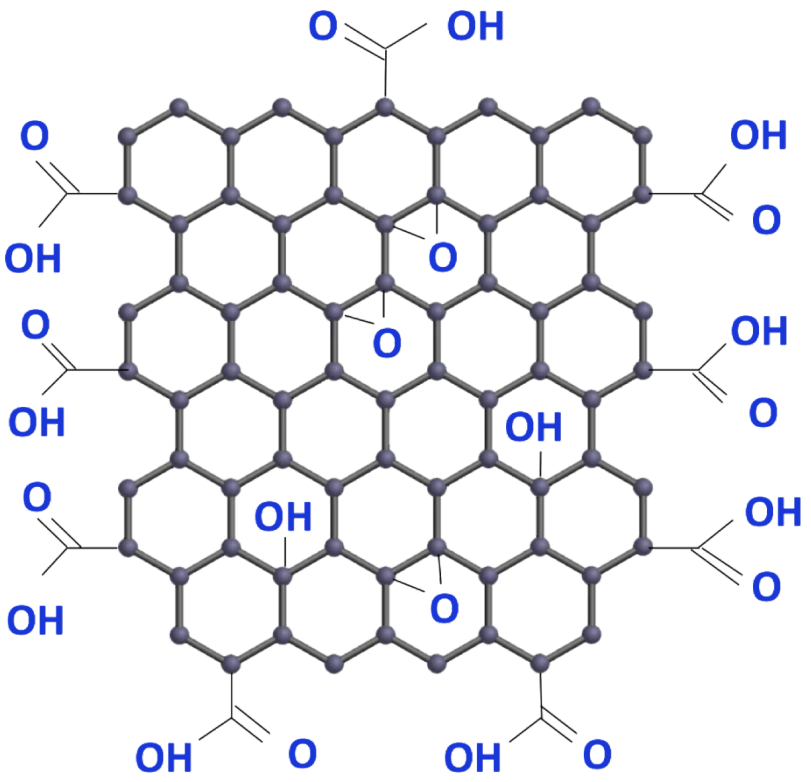


Figure 1.1 *The graphene oxide molecular structure consists of carbon, hydrogen and oxygen [63].*

Graphene oxide offers several advantages compared to other materials commonly used in energy storage including:

1. High Surface Area: GO possesses a high surface area, which is beneficial for energy storage applications such as supercapacitors, where it can provide increased charge storage capacity [33].
2. Electrical Conductivity: It exhibits good electrical conductivity, enabling efficient charge transport within energy storage devices, which is crucial for enhancing their performance [33].

3. Mechanical Flexibility: GO's mechanical flexibility is advantageous for applications in flexible electronics and energy storage systems that require conformal and bendable components [33].
4. Tunable Properties: The properties of GO can be tailored through surface modifications, making it a versatile material for a wide range of energy storage applications [34].

These points highlight the unique properties of graphene oxide that make it a promising material for energy storage applications, offering advantages over traditional materials in terms of surface area, electrical conductivity, mechanical flexibility, and tunable properties.
According to several review articles [33,34,35], the use of GO in energy storage devices has shown promising results, with improved performance compared to other materials commonly used in terms of charge storage capacity, power density, and stability. However, their performance can depend on several factors, such as the synthesis method and the quality of the material. Research indicates that optimizing the synthesis process of GO can lead to improved electrochemical properties, such as enhanced conductivity and capacitance. Additionally, the quality of the material, particularly in terms of reducing porosity to increase the active surface area, plays a crucial role in enhancing energy storage efficiency. Studies have shown that controlling the porosity of GO-based materials can significantly impact their performance in capacitors and batteries. By selecting appropriate synthesis methods and focusing on material quality, researchers can tailor GO-based energy storage devices with improved functionality and performance [36,34].

1.5.2 Key requirements for buffer layer

To fulfill energy storage applications effectively when employed as a buffer layer, GO should possess several key characteristics based on research and reviews:

1. Amphiphilicity: GO's ability to disperse in both water and various organic solvents enables versatile fabrication methods and compatibility with diverse substrates [38].
2. Stability: GO forms stable dispersions, ensuring consistent performance across multiple cycles [38].
3. Processability: Its aqueous processability facilitates scalable production techniques like drop casting [38].

4. Transparent conductivity: GO offers a balance between transparency and electrical conductivity, which is vital for optoelectronic applications like solar cells [38].
5. Electron mobility: Improving electron transport, while maintaining other desirable properties is important for enhancing overall device efficiency [38].
6. Controlled thickness: Precise control of the number of graphene layers ensures uniformity and optimizes performance [38].
7. Compatibility: GO must integrate seamlessly with other components within energy storage systems, such as electrolytes and electrodes [30,31].
8. Durability: High stability against degradation and excellent cycling performance are necessary for practical applications [38].

These attributes make GO a promising candidate for improving energy storage devices, particularly in areas where enhanced performance, flexibility, and sustainability are desired.

1.5.3 Synthesis techniques of graphene oxide

Graphene oxide can be synthesized by various methods, including the Hummers method, Tour's method, and modified Hummers methods. The Hummers method involves the oxidation of graphite with strong oxidizing agents in an acidic environment, but it is not environmentally friendly due to the evolution of NOx during the reaction. Modified Hummers methods, such as nitrate-free, two-step, co-oxidant, and low-temperature methods, have been developed to address this issue. Tour's method involves the use of phosphoric acid, sulfuric acid, and potassium permanganate. Additionally, GO can be synthesized using electrochemical and microbial methods [39,40]. The electrochemical method ensures better GO quality due to the use of aqueous electrolytes and the absence of oxidizing agents and reduced impurities. Furthermore, it is an environmentally friendly method because the electrolyte is re-used many times compared to other chemical methods [39]. The main disadvantages of the electrochemical method are the variability of the synthesis process as the synthesis conditions for pristine graphene, GO and graphene composites vary considerably, leading to process variability and also the need for specialized equipment and know-how for electrochemical synthesis [41,42]. On the other hand, the microbial method uses biological systems for the oxidation of graphite materials, offering an environmentally friendly approach to GO synthesis.

Other innovative methods for GO synthesis include mechanical exfoliation, epitaxial growth by chemical vapor deposition (CVD), and liquid-phase exfoliation. Mechanical exfoliation is a simple and environmentally friendly method, which produces high quality graphene with minimal defects, but has limited scalability for large scale production. Epitaxial growth by CVD allows precise control of the development process and is suitable for large scale production of high quality graphene, but requires specialized equipment and expertise, and has high installation costs [43]. Finally, liquid phase exfoliation is a relatively simple and economical method for the production of graphene dispersions. However, it may result in graphene of lower quality than other methods [43].

Bottom-up methods, such as CVD and epitaxial growth, can produce high-quality graphene oxide with fewer defects and impurities, but are more complex and time-consuming than top-down methods. Additionally, bottom-up methods may not be suitable for large-scale production of graphene oxide [45,46]. On the other hand, top-down methods are advantageous for their simplicity and ability to produce large quantities of graphene oxide. However, both methods have their limitations and are dependent on the specific application and desired properties of the graphene oxide [47,48].

Nevertheless, the advantages of top-down synthesis methods are suitable for applications that require large quantities of graphene oxide and where cost and scalability are important factors [46,48]. They are summarized below including:

1. Scalability: Top-down methods are often more scalable, allowing for the production of larger quantities of graphene oxide compared to bottom-up methods [48].
2. Simplicity: Top-down methods can be relatively simple and straightforward, requiring less complex processes and equipment for the production of graphene oxide [48].
3. Cost-Effectiveness: Some top-down methods can be more cost-effective for the large-scale production of graphene oxide, making them attractive for industrial applications [45].

The most commonly used top-down synthesis methods for graphene oxide include:

1. Chemical oxidation-reduction: This method involves the oxidation of graphite using strong oxidizing agents in an acidic environment, followed by reduction to form graphene oxide [45].
2. Arc discharge: This method involves the use of an electric arc to vaporize graphite, which then condenses into graphene oxide [45].

3. Exfoliation: This method involves the separation of graphene layers from graphite using mechanical, liquid-phase, or electrochemical methods [45].

Among these methods, the chemical oxidation-reduction has significant advantages including

1. Scalability: It is a scalable process that can produce large quantities of graphene oxide [49] without the use of toxic chemicals or high temperatures.
2. Cost-effectiveness: It is cost-effective compared to other top-down synthesis methods [49]. The method is relatively simple and versatile, allowing for the one-step preparation of electrochemically graphene oxide films on various substrates, such as glassy carbon electrodes, leading to enhanced electrochemical performance [52].
3. Control over properties: It allows the control over the properties of the graphene oxide produced, such as the number of layers and lateral size [49].
4. Ease of production: It is a relatively simple and straightforward process that does not require specialized equipment [50].

The quality of graphene oxide synthesized by the chemical oxidation-reduction method can vary depending on the specific conditions used during the synthesis process as follows:

1. Defects and impurities: It can result in defects and impurities in the graphene oxide, which can affect its properties [50]. However, the quality of graphene oxide produced by this method can be improved by optimizing the synthesis conditions and using high-quality starting materials.
2. Functional groups: It can introduce functional groups, such as hydroxyl, epoxy, and carboxyl groups, onto the surface of the graphene oxide [50]. These functional groups can enhance the mechanical, electrical, and chemical properties of the graphene oxide, making it suitable for various applications.
3. Layered structure: It can produce graphene oxide with a layered structure, which can be useful for applications that require the separation of individual layers [50].

1.7 References

[1] Koohi-Fayegh S. , Rosen M.A. , "A review of energy storage types, applications and recent developments",Journal of Energy Storage,27,101047,February 2020, https://doi.org/10.1016/j.est.2019.101047

[2] Chakraborty M.R, Dawn S.,Pradip Kumar S. , Bhusan Basu J. and Selim U.T.,"A Comparative Review on Energy Storage Systems and Their Application in Deregulated Systems",Batteries, 8(9), 124, September 2022, https://doi.org/10.3390/batteries8090124

[3] Ziad M. Ali,Martin Calasan ,Shady H. E. Abdel Aleem,Francisco Jurado and Foad H. Gandoman, "Applications of Energy Storage Systems in Enhancing Energy Management and Access in Microgrids:A Review",Energies,16(16),5930,August 2023, https://doi.org/10.3390/en16165930

[4] Zayed A. Shaqsi AL. , Sopian K. ,Al-Hinai A.,''Review of energy storage services, applications, limitations, and benefits",Energy Reports
6, Supplement 7, 288-306,December 2020, https://doi.org/10.1016/j.egyr.2020.07.028

[5] Types of energy storage, Nyserda.ny.gov, Available at:https://www.nyserda.ny.gov/All-Programs/Energy-Storage-Program/Energy-Storage-for-Your-Business/Types-of-Energy-Storage

[6] Chung D.D.L. ," Development, design and applications of structural capacitors" Applied Energy,231, Pages 89-101,1 December 2018, https://doi.org/10.1016/j.apenergy.2018.09.132

[7] Greenhalgh E. S., Nguyen S., Valkova M. ,Shirshova N., Milo S.P. Shaffer, Kucernak A.R.J. , "A critical review of structural supercapacitors and outlook on future research challenges",Composites Science and Technology
235,109968,12 April 2023,https://doi.org/10.1016/j.compscitech.2023.109968

[8] Karimi D.,Behi H.,Van Mierlo J. and Berecibar M.," A Comprehensive Review of Lithium-Ion Capacitor Technology: Theory, Development, Modeling, Thermal Management Systems, and Applications",Molecules,27(10), 3119, 12 May 2022, https://doi.org/10.3390/molecules27103119

[9] Abruna H.D.,Kiya Y.,Henderson J., C.,"Batteries and electrochemical capacitors:Present and future applications of electrical energy storage devices are stimulating research into

innovative new materials and novel architectures",Physics Today 61 (12), 43–47, 1 December 2008,https://doi.org/10.1063/1.3047681

[10] Treptow R.S.,"Lithium Batteries: A Practical Application of Chemical Principles",J. Chem. Educ.,80,9,1015,1 September 2003,https://doi.org/10.1021/ed080p1015

[11] Manthiram A., "A reflection on lithium-ion battery cathode chemistry", Nat. Commun. 11, 1550,25 March 2020, https://doi.org/10.1038/s41467-020-15355-0

[12] Gao J. et al,"Brief overview of electrochemical potential in lithium ion batteries",2016 Chinese Phys. B,25,018210,7 December 2015,DOI 10.1088/1674-1056/25/1/018210

[13] Sideris, P.J., Greenbaum, S.G.," Lithium Ion Batteries, Electrochemical Reactions" in. In: Brodd, R. (eds) Batteries for Sustainability. Springer, New York, NY,2013,https://doi.org/10.1007/978-1-4614-5791-6_8

[14] Asenbauer J. , Eisenmann T. , Kuenzel M. , Kazzazi A., Chen Z. , Bresser D. ,"The success story of graphite as a lithium-ion anode material – fundamentals, remaining challenges, and recent developments including silicon (oxide) composites", Sustainable Energy & Fuels,4,11 5387-5416,2020,https://doi.org/10.1039/D0SE00175A

[15] Goriparti, S., Miele, E., De Angelis, F., Di Fabrizio, E., Zaccaria, R. P., & Capiglia, C.," Review on recent progress of nanostructured anode materials for Li-ion batteries",Journal of power sources, 257, 421-443,1 July 2014,https://doi.org/10.1016/j.jpowsour.2013.11.103

[16] Ahn H., Kim, D., Lee, M. et al. "Challenges and possibilities for aqueous battery systems", Commun Mater 4, 37,26 May 2023, https://doi.org/10.1038/s43246-023-00367-2

[17] Kainatv S.,Anwer J., Hamid A.,Gull N., Maqsood K.S., "Electrolytes in Lithium-Ion Batteries: Advancements in the Era of Twenties (2020's)",Materials Chemistry and Physic,313,128796,1 February 2024,https://doi.org/10.1016/j.matchemphys.2023.128796

[18] Chang, Z., Li, C., Wang, Y. et al. "A lithium ion battery using an aqueous electrolyte solution", Sci Rep 6, 28421,22 June 2016, https://doi.org/10.1038/srep28421

[19] Chen S., Ring J.S.,Tao S.,"Key materials and future perspective for aqueous rechargeable lithium-ion batteries"Materials Reports: Energy,2, 2,100096,May 2022,https://doi.org/10.1016/j.matre.2022.100096

[20] Kaur G. and Byron D. Gates,"Review—Surface Coatings for Cathodes in Lithium Ion Batteries: From Crystal Structures to Electrochemical Performance" J. Electrochem. Soc. 169, 043504, 8 April,2022,DOI 10.1149/1945-7111/ac60f3

[21] Tan F.,An H.,Li N., Jun Du and Peng Z, "Stabilization of Li0.33La0.55TiO3 Solid Electrolyte Interphase Layer and Enhancement of Cycling Performance of

LiNi0.5Co0.3Mn0.2O2 Battery Cathode with Buffer Layer", Nanomaterials, 11(4), 989,12 April 2021, https://doi.org/10.3390/nano11040989

[22] Wei C., Yu C., Chen S., Chen S., Peng L.,Wu Y. Li S., Cheng S., Xie J., "Unraveling the LiNbO3 coating layer on battery performances of lithium argyrodite-based all-solid-state batteries under different cut-off voltages",Electrochimica Acta,438,141545,10,January 2023,https://doi.org/10.1016/j.electacta.2022.141545

[23] Jun J.Y ,Noh S. , Seong J.Y, Lee S. and Park Y.J, "Li3BO3-Li3PO4 Composites for Efficient Buffer Layer of Sulphide-Based All-Solid-State Batteries",Batteries, 9(6), 292,26 May 2023,https://doi.org/10.3390/batteries9060292

[24] Zhang D., Zhou Y., Liu C. and Fan S.,"The effect of the carbon nanotube buffer layer on the performance of a Li metal battery", Nanoscale, 8, 11161,28 April 2016,DOI: 10.1039/c6nr00465b

[25] Fan L. , Yanxia L., Enyang W., Jingjing R., Shimou C."Double-buffer silicon-carbon anode material by a dynamic self-assembly process for lithium-ion batteries",Electrochimica Acta,393,139041,10 October 2021, https://doi.org/10.1016/j.electacta.2021.139041

[26] Liu, Z., Du, J., Jia, H. et al., "Design of hierarchical buffer structure for silicon/carbon composite as a high-performance Li-ion batteries anode.",J Mater Sci: Mater Electron, 33, 3002–3015, 10 December 2022, https://doi.org/10.1007/s10854-021-07500-2

[27] Eigler S, Hirsch A. "Chemistry with graphene and graphene oxide-challenges for synthetic chemists.",Angew Chem Int Ed Engl.,53(30),7720-38,21 July 2014, doi: 10.1002/anie.201402780.

[28] Jiříčková A, Jankovský O, Sofer Z, Sedmidubský D.," Synthesis and Applications of Graphene Oxide.", Materials (Basel),15(3),920, 25 January 2022, doi: 10.3390/ma15030920.

[29] Wang Y.,Li S., Yang H. and Luo J., "Progress in the functional modification of graphene/graphene oxide: a review", RSC Adv., 10, 15328, 24 March 2020, DOI: 10.1039/d0ra01068e

[30] Yuheng T., Zhichun Y., Liuyue C., Li Zhang X., Chenghua S., Da-Wei Wang, "Graphene oxide: An emerging electro material for energy storage and conversion",Journal of Energy Chemistry, 55, 323-344,April 2021,https://doi.org/10.1016/j.jechem.2020.07.006.

[31] Dhamodharan D., Pradnya Prabhakar G., Veeman., Suhail M. Nidhin D., Hun S. B.,"A review on graphene oxide effect in energy storage devices",Journal of Industrial and Engineering Chemistry,106,20-36,25 February 2022,https://doi.org/10.1016/j.jiec.2021.10.033.

[32] Olabi A.G., Abdelkareem M.A, Wilberforce T., Sayed E.T,"Application of graphene in energy storage device – A review",Renewable and Sustainable Energy Reviews,135,January 2021,110026,https://doi.org/10.1016/j.rser.2020.110026.

[33] Zhu, J., Yang, D., Yin, Z., Yan, Q. and Zhang, H., "Graphene and Graphene-Based Materials for Energy Storage Applications." Small, 10,3480-3498, 15 January 2014, https://doi.org/10.1002/smll.201303202

[34] Xiaolu L., Ran M., Xiangxue W., Yan M., Yongping Y., Li Z., Sai Z., Riffat J., Jianrong C., Xiangke W.,"Graphene oxide-based materials for efficient removal of heavy metal ions from aqueous solution: A review",Environmental Pollution,252, Part A,62-73,September 2019,https://doi.org/10.1016/j.envpol.2019.05.050.

[35] Nouric E. Yu-Long W., Qian C., Jia-Ju X.,Paterakis G., Dracopoulos V, Zong-Xiang Xu, Tasis D., Mohammadi M.R, Lianos P.,"Introduction of Graphene Oxide as Buffer Layer in Perovskite Solar Cells and the Promotion of Soluble n-Butyl-substituted Copper Phthalocyanine as Efficient Hole Transporting Material",Electrochimica Acta,233,36-43,10 April 2017,https://doi.org/10.1016/j.electacta.2017.03.027

[36] Bagade, S.S.;Patel, S. Malik, M.M. Patel, P.K. "Recent Advancements in Applications of Graphene to Attain Next-Level Solar Cells." C-Journal of Carbon Research, 9, 70,19 July 2023, https://doi.org/10.3390/c9030070

[37] Lai, L. (2013). Energy storage applications of graphene-based materials. Doctoral dissertation,Nanyang Technological University, Singapore

[38] Velasco Davoise L, Díez-Pascual AM, Peña Capilla R. "Application of Graphene-Related Materials in Organic Solar Cells." Materials (Basel).15(3),1171,3 February 2022. doi: 10.3390/ma15031171.

[39] Jiříčková A, Jankovský O, Sofer Z, Sedmidubský D. "Synthesis and Applications of Graphene Oxide". Materials (Basel),15(3),920,25 January 2022,doi: 10.3390/ma15030920.

[40] Alam, S. , Sharma, N. and Kumar, L. "Synthesis of Graphene Oxide (GO) by Modified Hummers Method and Its Thermal Reduction to Obtain Reduced Graphene Oxide (rGO)*". Graphene, 6, 1-18, 1 January 2017, doi: 10.4236/graphene.2017.61001.

[41] F. Liu, C. Wang, X. Sui, M. Riaz, M. Xu, W. Liet al., "Synthesis of graphene materials by electrochemical exfoliation: recent progress and future potential", Carbon Energy, vol. 1, no. 2, 173-199, 2019, https://doi.org/10.1002/cey2.14

[42] Xiaohong S., Nan Y., Heng D., Han Y., Hongbing Y., Linya F.,

"In-situ electrochemical synthesis of heteroatoms-doped reduced graphene oxide toward nonradical degradation of tetracycline",Chemical Engineering Journal,471,144834
1 September 2023,https://doi.org/10.1016/j.cej.2023.144834.
[43] Adetayo A., Runsewe D., "Synthesis and Fabrication of Graphene and Graphene Oxide: A Review"Open Journal of Composite Materials, Vol.9 No.2,April 2019,DOI: 10.4236/ojcm.2019.92012
[44] Singh R. K. et al."Graphene oxide: strategies for synthesis, reduction and frontier applications", RSC Adv., 6 , 64993 —65011, 28 July 2016,DOI
https://doi.org/10.1039/C6RA07626B
[45] Gutiérrez-Cruz, A., Ruiz-Hernández, A.R., Vega-Clemente, J.F. et al." A review of top-down and bottom-up synthesis methods for the production of graphene, graphene oxide and reduced graphene oxide.", J Mater Sci 57, 14543–14578 ,6 August 2022.https://doi.org/10.1007/s10853-022-07514-z
[46] Vestince B. Mbayachi, Euphrem Ndayiragije, Thirasara Sammani, Sunaina Taj, Elice R. Mbuta, Atta ullah khan,"Graphene synthesis, characterization and its applications: A review," Results in Chemistry,3,100163,January 2021,https://doi.org/10.1016/j.rechem.2021.100163
[47] Al Jahdaly, B.A.; Elsadek, M.F.; Ahmed, B.M.; Farahat, M.F.; Taher, M.M.; Khalil, A.M. Outstanding Graphene Quantum Dots from Carbon Source for Biomedical and Corrosion Inhibition Applications: A Review." Sustainability, 13, 2127,17 February 2021, https://doi.org/10.3390/su13042127
[48] Kumar N., Salehiyan R., Vongani Chauke, Orebotse Joseph Botlhoko, Katlego Setshedi, Manfred Scriba, Mike Masukume, Suprakas Sinha Ray,
"Top-down synthesis of graphene: A comprehensive review",FlatChem, 27,100224,May 2021,https://doi.org/10.1016/j.flatc.2021.100224.
[49] Abbas Q, Shinde PA, Abdelkareem MA, Alami AH, Mirzaeian M, Yadav A, Olabi AG. "Graphene Synthesis Techniques and Environmental Applications." Materials (Basel). Nov 4,15(21),7804,2022, doi: 10.3390/ma15217804.
[50] Hu, Yang, Hanyu Gao, "Chemical synthesis of reduced graphene oxide: a review" Minerals and Mineral Materials. 2, no.3 8,2023 http://dx.doi.org/10.20517/mmm.2023.07
[51] Zhou A., Bai J., Hong W. Bai H.,
"Electrochemically reduced graphene oxide: Preparation, composites, and applications, Carbon,191,301-332,2022,https://doi.org/10.1016/j.carbon.2022.01.056.

[52] Qunpeng D., Lijie W., Fei W., Hongsong Z., Kui L.,"Facile One-Step Electrodeposition Preparation of Cationic Pillar[6]arene-Modified Graphene Films on Glassy Carbon Electrodes for Enhanced Electrochemical Performance" ,Frontiers in Chemistry,8 2020,DOI=10.3389/fchem.2020.00430

[53] Suranshe S.S., Patil A., Deshmukh T., Chavhan J.,"One step electrode fabrication of thin film graphene oxide-polypyrrole composite by electrodeposition using cyclic voltammetry for hybrid type supercapacitor application",Electrochimica Acta,450,142277,2023,https://doi.org/10.1016/j.electacta.2023.142277.

[54] Escobar-Teran F., Perrot H., and Sel O., "Carbon-Based Materials for Energy Storage Devices: Types and Characterization Techniques", Physchem 3, no.3, 355-384.13 September 2023, https://doi.org/10.3390/physchem3030025

[55] Gopalakrishnan K., Gurwinder S., Xinwei G., Jang M.L., Kavitha R., Stalin J., Mercy B., Ajay K., Jiabao Y., Prashant K., Ajayan V., "Recent Advances in Carbon-Based Electrodes for Energy Storage and Conversion",10, 18,2301045,25 April 2023, https://doi.org/10.1002/advs.202301045

[56] Zhiyong Q., Keyu B., Changming D., Yitao Z.,
"Recent progress of carbon-fiber-based electrode materials for energy storage",
Diamond and Related Materials,138,110208,Octrober 2023,https://doi.org/10.1016/j.diamond.2023.110208.

[57] Xu, Chaohe and Xu, Binghui and Gu, Yi and Xiong, Zhigang and Sun, Jing and Zhao, X. S.,"Graphene-based electrodes for electrochemical energy storage",
The Royal Society of Chemistry.6,5,1388-1414,2013,doi ="10.1039/C3EE23870A",

[58] Lee DK, Yoo J, Kim H, Kang BH, Park SH. Electrical and Thermal Properties of Carbon Nanotube Polymer Composites with Various Aspect Ratios. Materials (Basel). 2022 Feb 12;15(4):1356. doi: 10.3390/ma15041356.

[59] Gürten Inal II. Scalable activated carbon/graphene based supercapacitors with improved capacitance retention at high current densities. Turk J Chem. 2021 Jun 30;45(3),927-941. doi: 10.3906/kim-2012-39.

[60] Kim J., Kang J.G, Choi J., Paul V. Braun, and Kim S.K,"Fiber Electrodes Mesostructured on Carbon Fibers for Energy Storage", ACS Applied Energy Materials 2021 4 (12), 13716-13724,DOI: 10.1021/acsaem.1c02423

[61] Xinjun H., Enqi S., Bochao Z., Junji J., Peihong Y., Yongxiao B.,"Preparation of silanized graphene/poly(methyl methacrylate) nanocomposites in situ copolymerization and its mechanical properties",Composites Science and Technology, 97,6-11,2014,https://doi.org/10.1016/j.compscitech.2014.03.019.

[62] Sumin W., Lei Y., Qiguan W., Fan Y, J Shang J., Qiu S, Li J., Zhang W., Wu X.,,"Supramolecular self-assembly of layer-by-layer graphene film driven by the synergism of π–π and hydrogen bonding interaction",Journal of Photochemistry and Photobiology A: Chemistry, 355, 249-255,2018, https://doi.org/10.1016/j.jphotochem.2017.09.023.

[63] Graphene Oxide, ACS MATERIAL LLC
Nov 21, 2017, Available at : [https://www.acsmaterial.com/blog-detail/graphene-oxide.html]

CHAPTER 2. Synthesis-Experimental part

2.1 Synthesis of graphene oxide

The synthesis of GO was carried out by the modified Hummers method. The Hummers process is a chemical process used to produce graphite oxide, which can be further processed to obtain GO. The main chemical reaction involved in the Hummers method is the oxidation of graphite, which is achieved by introducing oxygen molecules into pure carbon. The reaction takes place between the graphene with the addition of concentrated sulphuric acid with potassium permanganate and sodium nitrate. Hydrogen peroxide is added at the end of the synthesis and its main role is to remove excess KMnO4, which stops the reaction. The chemical decomposition of GO is usually accompanied by a short reduction with the addition of hydrogen peroxide. Furthermore, the addition of hydrogen peroxide causes the synthesis of GO material and the opening of carbon chains. Additionally, it contributes to the widening of the graphene band gap through processes such as doping, intercalation and stripping of particles.

The Table 2.1 below shows the materials used for the synthesis of graphene oxide including the three main steps, which are oxidation, exfoliation and purification.

Materials	**Synthesis process**
Graphite powder (<20 μm)	Oxidation
Sulfuric Acid (H_2SO_4, 95-98%)	
Sodium nitrate ($NaNO_3$)	
Potassium permanganate ($KMnO_4$)	
Deionized water (H_2O)	Exfoliation
Hydrogen Peroxide (H_2O_2, 30%)	Purification

***Table 2.1**. Precursor materials for the three main steps of graphene oxide synthesis, oxidation, exfoliation and purification.*

The synthesis of the GO took two days to complete as indicated below:

1st Day:

1. 1 g of graphite and 46 ml of H_2SO_4 were placed in a 600 ml beaker.
2. The solution was stirred in an ice bath for 20 minutes.
3. 1 g $NaNO_3$ was slowly added in small quantities under continuous stirring for 1 hour.
4. 6 g $KMnO_4$ was carefully added to the solution with continuous stirring overnight.

Oxidation process

The chemical reactions that took place in the first step of oxidation are the following:

$$2NaNO_3\,(aq) + H_2SO_4\,(aq) \rightarrow 2HNO_3\,(aq) + Na_2SO_4\,(aq) \quad (1)$$

$$KMnO_4\,(aq) + H_2SO_4\,(aq) \rightarrow K^+ + MnO_3^+ + H_3O^+ + 3H_2SO_4^- \quad (2)$$

$$KMnO_4\,(aq) \rightarrow K^+\,(aq) + MnO_4^-\,(aq) \quad (3)$$

$$MnO_3^+\,(aq) + MnO_4^-\,(aq) \rightarrow Mn_2O_7\,(aq) \quad (4)$$

$$GIC\,(s) + Mn_2O_7\,(aq) \rightarrow \text{graphite oxide}\,(s) + \text{by-products} \quad (5)$$

These chemical reactions describe the oxidation of graphite to graphene oxide using different oxidizing agents. The first reaction involves the oxidation of graphite by $NaNO_3$ and H_2SO_4, leading to the intercalation of graphite and the formation of graphite oxide (Fig. 2.1).



Figure 2.1. *Oxidation of graphite by $NaNO_3$ and H_2SO_4.*

The subsequent reactions describe the oxidation of graphite by $KMnO_4$ and the formation of graphene intercalation compounds (GIC) and oxidizing agents such as Mn_2O_7. At this step, a change in color of the solution to green was observed due to the dissolution of $KMnO_4$ to MnO_4^- (Fig. 2.2). The overall oxidation process took 24 hours.



Figure 2.2. *Color change of the solution to green after the addition of $KMnO_4$.*

In summary, the oxidation of graphite to graphene oxide involves the intercalation of graphite by the oxidizing agents, which leads to the formation of graphite intercalation compounds (GIC), and ultimately, the production of graphite oxide. The presence of strong oxidants, such as $NaNO_3$ and $KMnO_4$, enhances the oxidation process and leads to the formation of oxidizing agents that facilitate the oxidation of graphite [1,2,3].

2nd Day

Exfoliation and Purification process

The reactions, which took place at the step of exfoliation and purification (2nd day) of graphene oxide, are the following:

$5H_2O_2\ (aq) + 2KMnO_4\ (aq) + 3H_2SO_4\ (aq)$

$\rightarrow 5O_2\ (g) + MnSO_4\ (aq) + K_2SO_4\ (aq) + 8H_2O\ (l)$ (6)

$H_2O_2\ (aq) + HNO_3\ (aq) \rightarrow HNO_4\ (aq) + H_2O\ (l)$ (7)

$2MnO_4^-\ (aq) + 5H_2O_2\ (aq) + 6H^+\ (aq) \rightarrow 2Mn^{2+}\ (aq) + 8H_2O\ (l) + 5O_2\ (g)$ (8)

1. The solution was heated at 35 °C and stirred for 1 hour, followed by stirring for 40 minutes.
2. Subsequently, the temperature was increased to 90 °C, and 80 ml of DIH_2O was added very slowly under stirring conditions for 40 minutes (Fig. 2.3).

At this point, it is worth noting that when water was added to the original solution, a color change to brown was observed due to the formation of oxygen-containing functional groups in the graphite layers. These functional groups include carboxyl (-COOH), epoxide (-O-) and hydroxyl (-OH) groups, which interrupt the continuous aromatic lattice of the pristine graphite and render GO hydrophilicity [1].



Figure 2.3 *Color change of the solution to brown after the addition of 80 ml DIH_2O.*

3. After 40 minutes, the heat was turned off, and 200 ml of DIH_2O was added (Fig. 2.4).



Figure 2.4 *Color change of the solution to yellow after the addition of 200 ml* DIH_2O.

The yellow color represents the complete introduction of the functional groups (carboxyl (-COOH), epoxide (-O-) and hydroxyl (-OH) groups) into the pristine graphite lattice leading to the conclusion that the synthesis of the graphene oxide has been completed.

4. 20 ml of H_2O_2 was slowly added to the solution with continued stirring until room temperature was reached (Fig. 2.5).



Figure 2.5 *Solution after the addition of* H_2O_2 *to remove impurities.*

H_2O_2 was added to the solution acting as a reducing agent to remove oxidizing impurities. The success of the process was confirmed with the change in color (i.e. the darker it becomes the freer of impurities it is).

5. The entire solution was centrifuged at 9000 rpm for 5 minutes.

6. 200 ml of DIH_2O was heated at 65 °C for washing the sediment after centrifugation.

7. The centrifugation and washing of the sediment were repeated three times using approximately 90 ml of warm water each time.

8. The sediment was washed off with cold DIH_2O until the pH was 7 and checked with pH strips.

9. The GO sediment was dried in the oven at 60 °C for about 4 days (Fig. 2.6).



***Figure 2.6**. The GO flakes.*

10. The dried GO was pulverized with a pestle and mortar until a fine powder formed and stored in 40 ml vials for further use (Fig 2.7).



Figure 2.7 *The GO powder.*

The processes aim to ensure that the graphene oxide is free of any by-products from the previous reactions and is ready for storage and future use.

2.2 The preparation of graphene oxide dispersion

After the synthesis of the GO, its dispersion in water was prepared. This prepared solution was then used for the electrodeposition of the material on the substrate as described in the following sections. The steps for the preparation of the dispersion were:

1. 80 mg of GO was weighed.
2. Then 40 ml of DIH_2O was added in a 40 ml glass vial.
3. The solution was then placed on a hot plate at 50 °C for 24 hours under stirring for homogenization (Fig. 2.8).
4. The solution was then placed on an ultrasonic probe to achieve dispersion for 30 minutes in an ice bath to avoid overheating (Fig. 2.9).
5. Finally, it was centrifuged at 9000 rpm for 5 minutes.
6. The final solution was collected from the suspension after centrifugation.

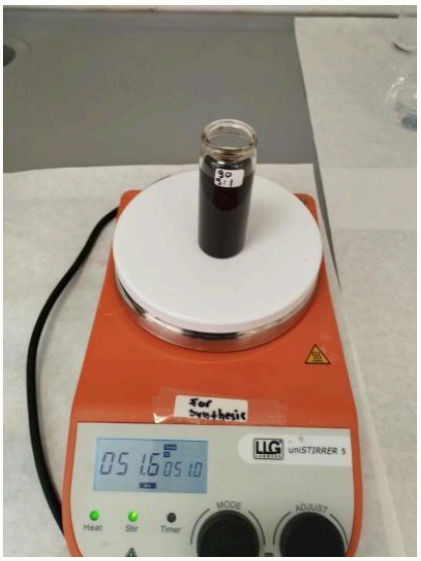


Figure 2.8 *The homogenization of the GO solution.*

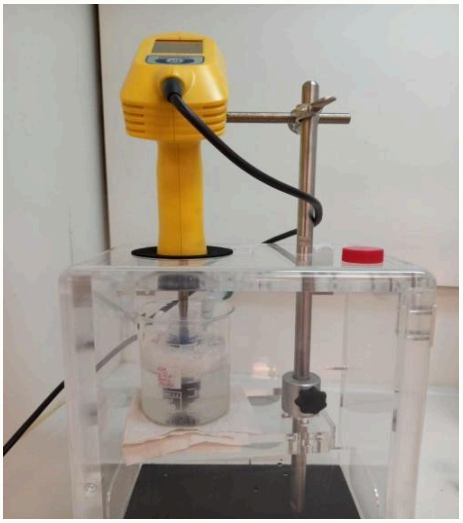


Figure 2.9 *The GO dispersion through the ultrasonic probe.*

2.3 Substrates

Copper substrates were used for the deposition of GO on the top of them. The protocol followed for cleaning the substrates was

1. Firstly, the copper substrates were cut into specific dimensions (1*1 cm) and polished to remove any impurities.
2. Then, they were placed in a beaker with the addition of soapy water and transferred in an ultrasonic bath for 10 minutes.
3. They were then rinsed with DIH_2O.
4. Acetone was added to the beaker with the substrates and transferred in the ultrasonic bath for another ten minutes.
5. The acetone was then removed and isopropanol was added to the beaker and placed back in the ultrasonic bath for ten more minutes.
6. Finally, the copper substrates were dried using a nitrogen gas gun.

2.4 The electrodeposition of graphene oxide buffer layers

For the synthesis of graphene oxide by the electrodeposition method, the Metrohm Autolab potentiostat/galvanostat device was used (Fig. 2.10).



Figure 2.10 *The Metrohm Autolab potentiostat/galvanostat system.*

The synthesis of the electrodes was carried out with a three-electrode connection as shown in Figure 2.11. Silver/silver chloride (Ag/AgCl) electrode, graphite foil and copper substrate were used as the reference, counter and working electrode, respectively. These three electrodes were embedded in the graphene oxide solution during a stirring deposition process. The first set of samples included the current parameter (0.25 mA/cm^2) constant, while changing the deposition time (3, 5 and 10 min). Then, by selecting the material for 3-min

deposition time with the best adhesion, the effect of electrolyte with different concentrations (0.1, 0.5 and 1 M) as well as the different ratio of graphene oxide (2:1 and 3:1 GO:H_2O) during the synthesis were further investigated. Table 2.2 below shows the different samples prepared with the parameters used. Finally, the samples were dried in an oven at 65 ºC for 15 minutes. The prepared layers were analyzed structurally, morphologically and electrochemically.

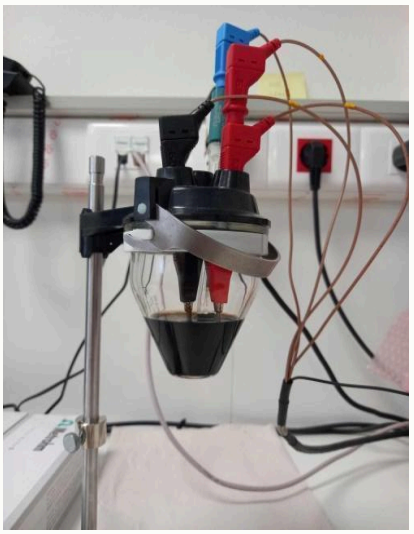


Figure 2.11 *The three-electrode electrochemical cell consisted of the Ag/AgCl (blue) as reference, the graphite as counter (black) and the Cu substrate as working electrode (red) along with the dispersed GO solution as electrolyte.*

Samples	Deposited Current	Deposited Time	Electrolyte Concentration (Li_2SO_4)	Ratio of Graphene oxide/H_2O
1st set of experiment				
1st	0.25 mA/cm^2	**3 min**	01 M	2:1
2nd	0.25 mA/cm^2	**5 min**	0.1 M	2:1
3rd	0.25 mA/cm^2	**10 min**	0.1 M	2:1
2nd set of experiment				
4th	0.25 mA/cm^2	3 min	**0.5 M**	2:1
5th	0.25 mA/cm^2	3 min	**1 M**	2:1
3rd set of experiment				
6th	0.25 mA/cm^2	3 min	0.1 M	**3:1**
4th set of experiment				
7th	**0.5 mA/cm^2**	5 min	0.1 M	2:1
8th	**0.75 mA/cm^2**	5 min	0.1 M	2:1

Table 2.2 *The series of samples performed and the parameters (bold) changed in each series including deposition time, electrolyte concentration, GO:H_2O ratio and deposition current.*

2.5 Characterisation techniques

2.5.1 Raman spectroscopy

Raman spectroscopy is a non-destructive analytical technique that uses scattered light to measure the vibrational energy modes of a sample. It provides detailed information about chemical structure, phase, crystallinity, and molecular interactions. Raman spectroscopy relies on the interaction of light with the chemical bonds within a material, and it can be used to analyze solids, powders, slurries, liquids, gels, and gasses. It can provide both chemical and structural information, as well as the identification of substances through their characteristic Raman 'fingerprint'. It can be used in many fields, including chemistry, biology, medicine, and materials science. At least 25 variations of Raman spectroscopy have been developed, including surface-enhanced Raman, Raman microscopy, and resonance Raman [4].

Raman spectroscopy is a powerful technique for characterizing GO and its derivatives, providing insights into the material's quality and structure. GO exhibits distinct Raman peaks

compared to pristine graphene, such as the D peak (around 1350 cm^{-1}) and the G peak (around 1580 cm^{-1}). The D peak is associated with defects and disorder in the graphene lattice, while the G peak is related to the in-plane vibrations of sp^2-bonded carbon atoms [4,5,6].

The Raman spectrometer system requires three primary components: a high-intensity laser, a sample interface, and a spectrometer. The laser acts as the excitation source, providing the high-intensity light required to obtain sufficient Raman signals for detection. The sample interface directs and focuses the incident beam and collects the weak Raman emissions for routing to the spectrometer. The spectrometer captures and detects all the light transmitted by the sample interface, reporting a spectrum as a function of Raman shift relative to the laser frequency.

Raman measurements of the samples in this study were obtained at room temperature with a Thermo Fisher Scientific DXRxi system. The parameters used were:

1. Laser source: 532 nm
2. Lens Slit: x50
3. Laser power: 10 mW
4. Exposure time: 0.1 s (10 Hz)

2.5.2 Scanning electron microscopy/Dispersive X-ray spectroscopy

Scanning electron microscopy (SEM) and energy dispersive X-ray spectroscopy (EDS) are techniques used for targeted analysis of sample surfaces. SEM provides detailed high-resolution images of the sample by rastering a focused electron beam across the surface and detecting secondary or backscattered electron signals. EDS is used to provide elemental identification and quantitative compositional information. It is possible to take advantage of the physical interactions that occur at the sample surface to obtain chemical information. The principle of the SEM is based on a cathode ray tube in which electrons are produced in the cathode by passing a current through a metal filament. The generated electrons are then accelerated towards the anode using high voltage. At the anode, the electron beam is concentrated through a series of thin apertures and electromagnetic fields are created that surround the column. The electron beam eventually exits the column directed towards the surface of the sample. As the electron beam adsorbs on the sample, various physical phenomena such as secondary electron generation takes place. Secondary electrons are

produced by the sample itself, which is attributed to the electron energy of the incident beam. The secondary electrons are "collected" by an off-axis detector that uses the secondary electron to fluoresce a scintillating material on the surface of the detector, much as a cathode ray tube uses phosphorus to fluoresce on a television screen. The fluorescent material on the face of the detector is then translated into an electronic signal using a photomultiplier tube. The position of this electronic signal is determined by 'scanning' the sample with the electron beam and the detector signal is linked to that of the position of the incident beam. As secondary electrons are produced for imaging, the interacting atom is ionized and a photon is emitted that carries energy corresponding to the electronic transition, according to the laws of quantum mechanics. The EDS detector is a tool used to measure this energy of emitted photons through x-rays. The detected. X-rays are separated into energy channels based on their interaction with the detector and form a spectrum of detected energies. With the spectrum, the maximum energies can be identified and it can be determined which electron transition has taken place and thus to which element it corresponds.

These techniques are widely used for material surface analysis, investigation of product failures, reverse engineering, contaminant identification, solder joint analysis, and more [7,8]. The combination of SEM and EDS offers several advantages for materials analysis and failure investigation [7,8]:

1. High-resolution imaging and chemical analysis: SEM provides detailed images of sample surfaces, while EDS allows for elemental identification and quantitative compositional information.
2. Versatility: SEM/EDS is applicable to a wide range of industries and materials, including metals, polymers, ceramics, and composites.
3. Non-destructive analysis: SEM/EDS is typically non-destructive, which means that samples can be analyzed without being damaged.
4. Accuracy: SEM/EDS provides precise chemical information about samples on very small scales.
5. Sensitivity: EDS is sensitive to low concentrations, making it useful for detecting trace elements.
6. Speed: SEM/EDS can provide quick elemental analysis, which is beneficial for time-sensitive applications.
7. Automation: Modern SEM/EDS systems are equipped with automation features that can save time and improve efficiency.

8. Integration: SEM/EDS systems are often integrated, which means that users can obtain both imaging and chemical data from the same instrument.

For the morphological analyses of the samples a Field Emission Scanning Electron Microscope (FE-SEM) as developed on the JSM-IT700HR InTouchScope™ Field Emission SEM (Thermo Fisher Scientific) with 10 kV up to 20 kV power and 9.8 μm width was used collecting several magnifications (from x1,500 to x50,000). All samples were subjected to Au sputtering for 39 seconds before being placed in the microscope due to graphene oxide fluorescence. The cross section was made at an angle of 90°, moving the holder to a vertical position.

2.5.3 X-Ray photoelectron spectroscopy

X-ray photoelectron spectroscopy (XPS) is a surface-sensitive quantitative spectroscopic technique used to analyze the elemental composition of a material's surface, as well as its chemical state and electronic structure. XPS is based on the photoelectric effect, in which soft X-rays are used to eject electrons from the sample, where the kinetic energy and number of ejected electrons are measured to determine the chemical states of the elements present. XPS requires high vacuum or ultra-high vacuum conditions, and can detect all elements except hydrogen and helium. It is a powerful measurement technique because it shows what elements are present and how they are bonded. The technique can be used in line profiling of the elemental composition across the surface, or in depth profiling when paired with ion-beam etching [9].

XPS has been used to analyze GO and its composites, providing valuable information about their chemical composition and structure. It is a quantitative and reliable technique that uses X-rays to remove electrons from the C 1s and O 1s levels of graphene and related materials, allowing the determination of elemental composition in the parts-per-thousand range and the nature of chemical bonds [10].

For the measurements accomplished in this work, a monochromatic Al-K_a source in FlexMod (SPECS-SPECS Surface Nano Analysis GmbH) with an XR-50 X-ray source and 15kV/200 W was used.

2.5.4 Cyclic voltammetry

Cyclic voltammetry (CV) is an electrochemical technique used to investigate the redox properties of molecules in solution. It involves cycling the potential of a working electrode, while measuring the resulting current. This technique is commonly used to study redox processes, determine reaction kinetics, and investigate the stability of reaction products. CV is performed using a three-electrode system consisting of a working electrode, a reference electrode, and a counter electrode, as shown in Figure 2.12. The resulting data is plotted as current versus applied potential, yielding a characteristic plot known as a cyclic voltammogram (Fig. 2.13). CV is a powerful and widely used method in electrochemistry, providing valuable information about the electrochemical behavior of various compounds [11].

Some specific applications of cyclic voltammetry include:

1. Studying the redox behavior of analytes and their stability.
2. Determining the presence of intermediates in redox reactions.
3. Investigating electron transfer kinetics.
4. Measuring the diffusion coefficient of an analyte.
5. Determining the formal reduction potential of an analyte, which can be used as an identification tool.
6. Quantitative analysis of chemical species in solution.
7. Studying the electrochemical behavior of working electrode surfaces.
8. Investigating the reversibility of reactions.
9. Determining the electron stoichiometry of a system.

Cyclic voltammetry is a versatile technique that can be used in various fields, including analytical chemistry, materials science, and electrochemistry. It is a valuable tool in battery research, particularly in the investigation of lithium-ion batteries. It provides essential information about the redox properties, charge-discharge mechanisms, and electrochemical stability of materials used in batteries. By analyzing the battery properties, CV can help in tuning the battery reaction mechanisms, studying the influence of electrolyte concentration, investigating the effect of electrode thickness, and understanding the impact of temperature on battery performance. This technique is used to evaluate the behavior of various battery components, such as electrolytes, anode and cathode materials. For instance, in the case of

electrodes, CV can be utilized to probe the reactions of the electrode, assess the formation of the Solid Electrolyte Interface (SEI), and provide information about charge transfer processes. Additionally, CV can help in identifying reduction and decomposition products, as well as in evaluating the safe voltage range for battery materials. Overall, CV is a fundamental tool in battery research [12].



Figure 2.12 *The three-electrode electrochemical cell consisted of the reference Ag/AgCl(blue), the counter graphite (black) and the working electrode being the synthesized sample on Cu (red) with* Li_2SO_4 *acting as electrolyte.*

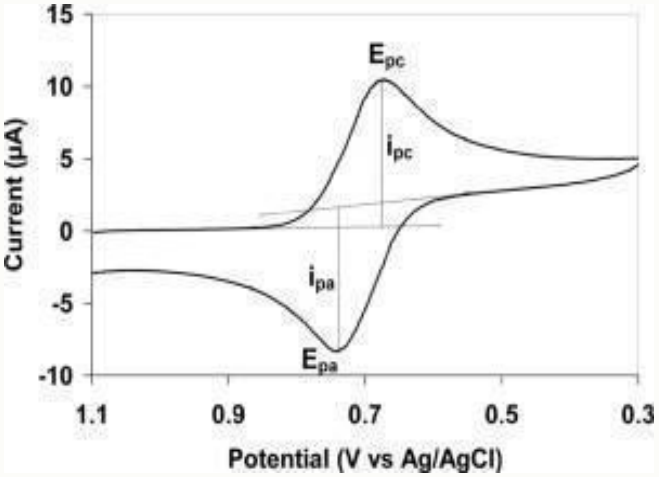


Figure 2.13 *Typical cyclic voltammogram where* i_{pc} *and* i_{pa} *show the peak cathodic and anodic current, respectively for a reversible reaction [13].*

2.6 References

[1] Chen X. Zhan Qu, Liu Z., and Ren G., "Mechanism of Oxidation of Graphite to Graphene Oxide by the Hummers Method",ACS,Omega,7,27 23503-23510,2022,DOI: 10.1021/acsomega.2c01963

[2] Lakhe P., Devon L. Kulhanek, Zhao X., Papadaki M. I., Majumder M., and Green M. J., "Graphene Oxide Synthesis: Reaction Calorimetry and Safety", Industrial & Engineering Chemistry Research,59,19, 9004-9014,
2020,DOI: 10.1021/acs.iecr.0c00644

[3] Tarko F.E. & Delele Worku A., "Controlled synthesis, characterization and reduction of graphene oxide: A convenient method for large scale production", Egyptian Journal of Basic and Applied Sciences, 4:1, 74-79, 2017, DOI: 10.1016/j.ejbas.2016.11.002

[4] Raman C., Krishnan K. "A New Type of Secondary Radiation", Nature 121, 501–502 1928, https://doi.org/10.1038/121501c0

[5] Diez-Betriu X. and Alvarez-Garc G.,Botas, Cristina and Alvarez, Patricia and Sanchez-Marcos, Jorge and Prieto, Carlos and Menendez, Rosa and de Andres, Alicia", "Raman spectroscopy for the study of reduction mechanisms and optimization of conductivity in graphene oxide thin films",J. Mater. Chem. C,1,41,6905-6912,2013,doi =10.1039/C3TC31124D

[6] López-Díaz D., Delgado-Notario J.A., Clericò V., Diez E., Dolores Merchán M., and Mercedes Velázquez M., "Towards Understanding the Raman Spectrum of Graphene Oxide: The Effect of the Chemical Composition" Coatings 10, no. 6,
524,2020,https://doi.org/10.3390/coatings10060524

[7] Asif A., Zhang N., and Santos R.M. "Mineral Characterization Using Scanning Electron Microscopy (SEM): A Review of the Fundamentals, Advancements, and Research Directions" Applied Sciences 13, no. 23, 12600,2023,https://doi.org/10.3390/app132312600

[8] Abd Mutalib M. , Rahman M.A., Othman M.H.D. , Ismail A.F., Jaafar J. ,"Scanning Electron Microscopy (SEM) and Energy-Dispersive X-Ray (EDX) Spectroscopy",Elsevier,Chapter
9,161-179,2017,https://doi.org/10.1016/B978-0-444-63776-5.00009-7

[9] Greczynski G., Hultman L.,"X-ray photoelectron spectroscopy: Towards reliable binding energy referencing",Progress in Materials
Science,107,100591,2020,https://doi.org/10.1016/j.pmatsci.2019.100591

[10] Kovtun, A., Jones, D., Dell'Elce, S. et al, "Accurate chemical analysis of graphene-based

materials using X-ray photoelectron spectroscopy". Carbon, 143, 268-275, 2019, http://dx.doi.org/10.1016/j.carbon.2018.11.012

[11] Elgrishi, Noémie,Rountree, Kelley J.,McCarthy, Brian D.Rountree, Eric S.Eisenhart,,Thomas T.,Dempsey, Jillian L., "A Practical Beginner's Guide to Cyclic Voltammetry", J. Chem. Educ., 95, 2, 197–206,3 November,2017,https://doi.org/10.1021/acs.jchemed.7b00361

[12] Cometto C. et al., "Means of Using Cyclic Voltammetry to Rapidly Design a Stable DMC-Based Electrolyte for Na-Ion Batteries". Journal of The Electrochemical Society, 166,15, 2019,DOI 10.1149/2.0721915jes

[13] Saad A., Tonello S., Borghetti M., Sardini E., Serpelloni M., "Potentiostats for Protein Biosensing: Design Considerations and Analysis on Measurement Characteristics", Journal of Sensors, 2019,20,6729329, 2019, https://doi.org/10.1155/2019/6729329

CHAPTER 3. The effect of deposition time on the synthesis of graphene oxide

3.1 Introduction

This chapter presents the results of the structural, morphological and electrochemical characterisation of the first series of samples. The aim is to investigate the growth mechanism of the material using the electrodeposition technique and evaluate its impact on the electrochemical performance of GO. In this series of experiments, the deposition current was constant at 0.25 mA/cm^2 for 3, 5 and 10 min. The growth mechanism of the material in correlation with the deposition time was studied and the basic characterization of structure, morphology and electrochemical behavior of the synthesized materials was performed. The characterization measurements carried out, were Raman spectroscopy to confirm the presence of graphene oxide, SEM to obtain information on the morphology of the samples and their thickness for the estimation of the growth mechanism, XPS to investigate the chemical elements and their bonds, and CV to study their electrochemical behavior and stability in continuous cycles of intercalation and deintercalation.

3.2 Raman Spectroscopy Results

The Raman spectra for the first set of samples are shown in Figure 3.1. The D and G bands in the Raman spectrum of GO are significant indicators of the material's structural properties and the degree of oxidation. The D band, also known as the disorder band or the defect band, is associated with structural defects, edge effects, and dangling sp^2 carbon bonds that break the symmetry. The D band is typically found at a lower wavenumber (around 1350 cm^{-1}) compared to the G band. The G band, on the other hand, is the primary mode in graphene and graphite, representing the planar configuration of sp^2 bonded carbon [2,3]. The G band is found at a higher wavenumber (around 1582 cm^{-1} for graphite) and is resonant, meaning it is much more intense than expected [2,3].

The intensity ratio of the D and G bands (I_D/I_G) in GO is higher than that of pristine graphite, which confirms the presence of defects and functional groups introduced during the oxidation process [4]. This ratio is a useful tool for understanding the material's structural properties and the degree of oxidation. A higher I_D/I_G ratio indicates an increased degree of disorder and defects, while a lower ratio indicates a higher degree of graphitization upon reduction. The intensity ratio of the D and G bands (I_D/I_G) in GO is typically around 1, indicating a moderate level of defects in the material. However, the exact value can vary depending on the specific sample and its degree of reduction or defect concentration. For example, the I_D/I_G ratio has been reported to be around 1.08 for reduced graphene oxide (rGO) [4], and it can increase to around 2.5 for more defective samples [5]. In this work, it was found to be close to 1 in all samples, suggesting that the degree of disorder of the prepared graphene structure is relatively low (Figure 3.2). Additionally, from Figure 3.1, one can observe that the sample with 0.25 mA/cm^2 for 3 min deposition time may have better crystallinity than the others with longer times due to the fact that the peak intensities are higher and the peak widths are narrower.

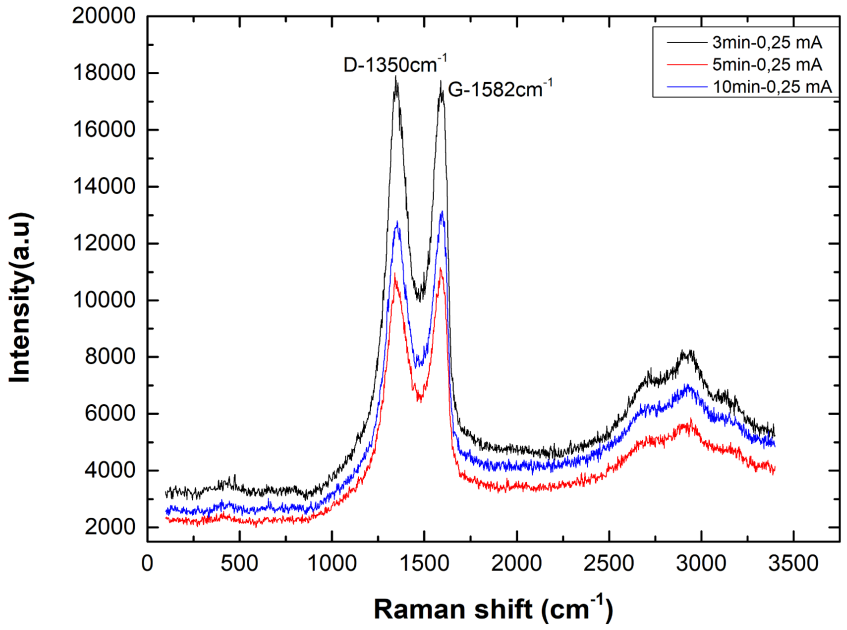


Figure 3.1 *Raman spectra of synthesized samples with a constant deposition current density of 0.25 mA/cm^2 at different deposition times of 3 minutes (black line), 5 minutes (red line) and 10 minutes (blue line).*

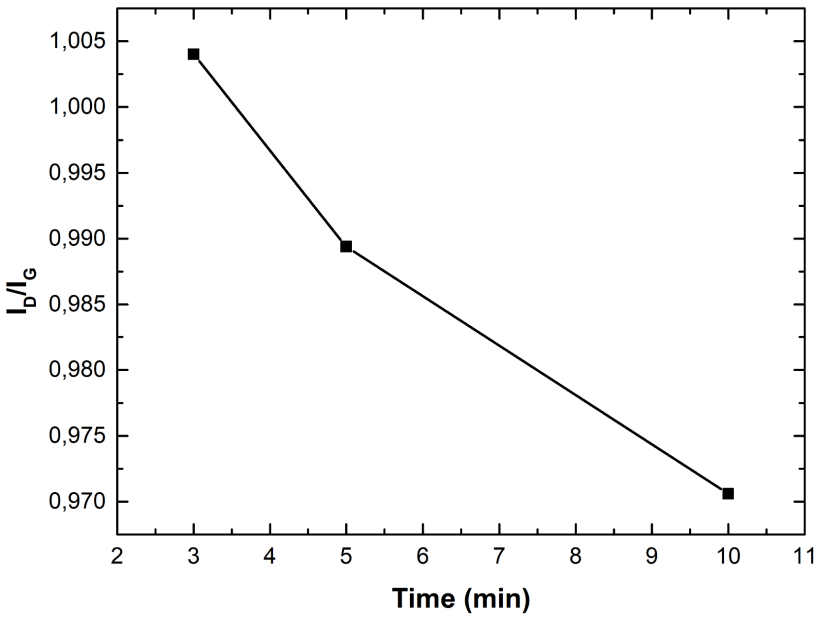


Figure 3.2 *The diagram of the I_D/I_G ratio as a function with the different deposition times.*

3.3 SEM Results

In order to investigate the growth of GO in relation to deposition time and its impact on the materials morphology, SEM images were obtained. As can be seen in Figure 3.3, a more homogeneous structure is observed for the shorter deposition time, compared to the longer periods. In addition, the samples with longer deposition times seem to form agglomerations, which is in agreement with the Raman results (having lower intensity). These agglomerations probably affect the adhesion of graphene oxide on the copper substrate, causing cracks.

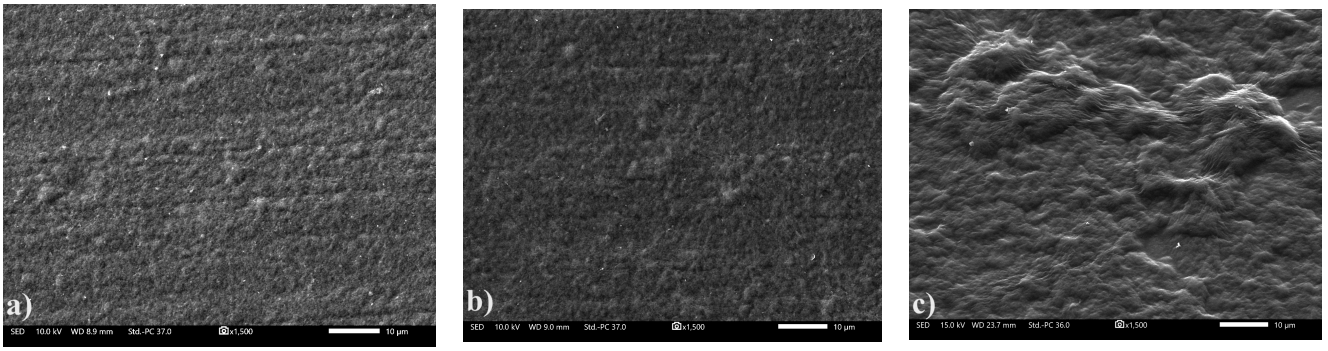


Figure 3.3 *SEM images of a) 3 min, b) 5 min, c) 10 min deposition time of GO on Cu substrate with 0.25 mA/cm^2 deposition current density. The magnification in all images is x 1500 and the line is equal to 10 μm.*

In the following Figure 3.4, the cross-section SEM analysis of the samples was performed to estimate their thickness. Table 3.1 shows the thickness of the samples with different deposition time. There is limited information on how the thickness of GO affects its properties. However, some studies have investigated the evolution of graphene properties during in-plane growth of graphene from RGO on Cu via CVD. The results showed a monotonous enhancement of the structural quality of the graphene with increasing length of the graphene from RGO [6]. Another study investigated the nucleation and growth mechanism of tin electrodeposition on GO and found that the morphology and structure of the deposited tin were affected by the concentration of GO and the deposition time [7]. Additionally, according to the literature, the optimization of effective parameters for electrodeposition of graphene oxide, such as concentration, pH, scan rate, and number of cycles, have shown to minimize charge transfer resistance [8]. The above data underscore the critical role of adjusting processing parameters in enhancing material performance. In this work, it is clear that the deposition time affects the thickness of the material since it is lower for longer periods (Table 3.1). This is possibly due to the agglomerates formed in the GO matrix, which prevent the growth of the material on the substrate (Figure 3.3).

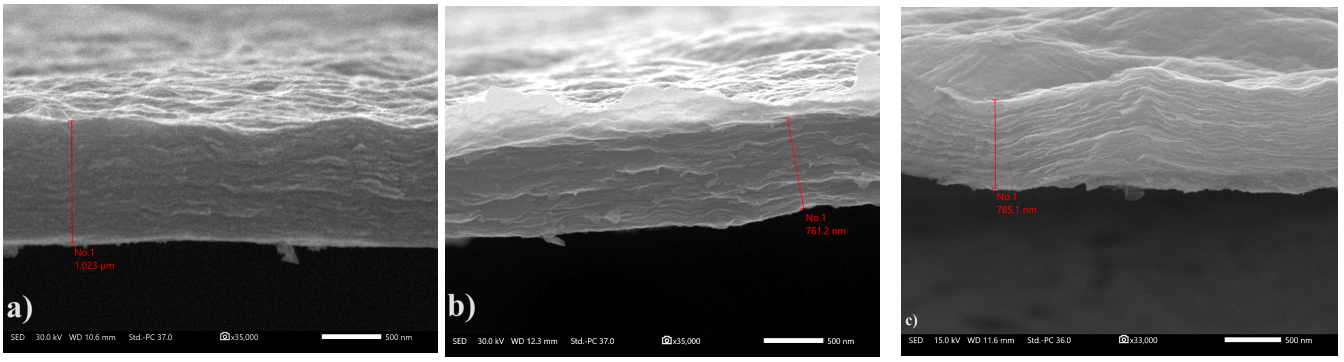


Figure 3.4 *The cross-section SEM analysis of the samples a) 3 min, b) 5 min, c) 10 min deposition time with 0.25mA/cm² deposition current density. The magnification is x15,000 and the line is equal to 500 nm.*

Deposition time	Thickness (nm)
3 min	1023
5 min	761,2
10 min	785,1

Table 3.1 *The thickness of electrodeposited GO for deposition time 3 min,5 min and 10 min with* 0.25 mA/cm^2 *current density.*

3.4 XPS Results

In order to further investigate the structure of GO in relation to deposition time, XPS measurements were obtained. All analyses of the XPS spectra were performed with Origin.Pro vol.9 software through Gaussian non-linear fitting and baseline normalization of the peaks. In Figure 3.5 the XPS spectrum of the GO sample for 3 min deposited time with 0.25 mA/cm^2 current density is shown. As can be observed, graphene oxide shows four peaks. The peaks around ~284.6 eV are attributed to the C-C and C=C lattices of graphene. The epoxy and phenolic -OH-bonded carbons show relative binding energy at ~286.6 eV, while the corresponding signals of ketone, lactone and carboxyl-containing carbons are at ~290,3 eV. The signals of carbons from ketone groups located in the defect regions of the GO samples are located at ~285.8 eV, which are also verified through the literature [9].

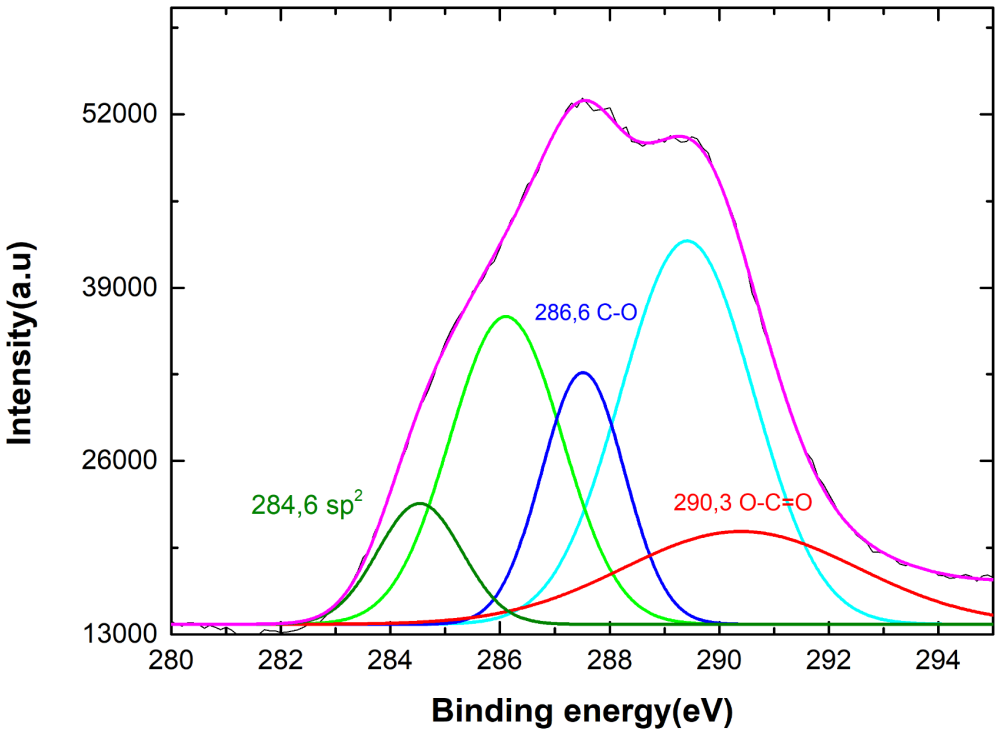


Figure 3.5 *C1s XPS spectra of the sample for 3 min deposition time with 0.25 mA/cm^2 deposition current density.*

In Figure 3.6, the results from O1s spectra of GO samples confirm the C1s results according to which the graphite structure is strongly oxidized and contains different oxygen functionalities. Therefore, the signal around ~530 eV corresponds to the bonds O=C-OH, ~532 eV attributes to C-O and O–C=O from carboxylic group and the signal around ~535,2 eV corresponds to phenolic –OH and epoxy groups. O1s XPS shows qualitatively that during reduction some amount of oxygen functionalities remain on the surface. They are mainly phenolic hydroxyl groups and epoxy groups. The reason for their incomplete reduction could be explained with the existence of oxidative by-products on the surface of graphene oxide [10].

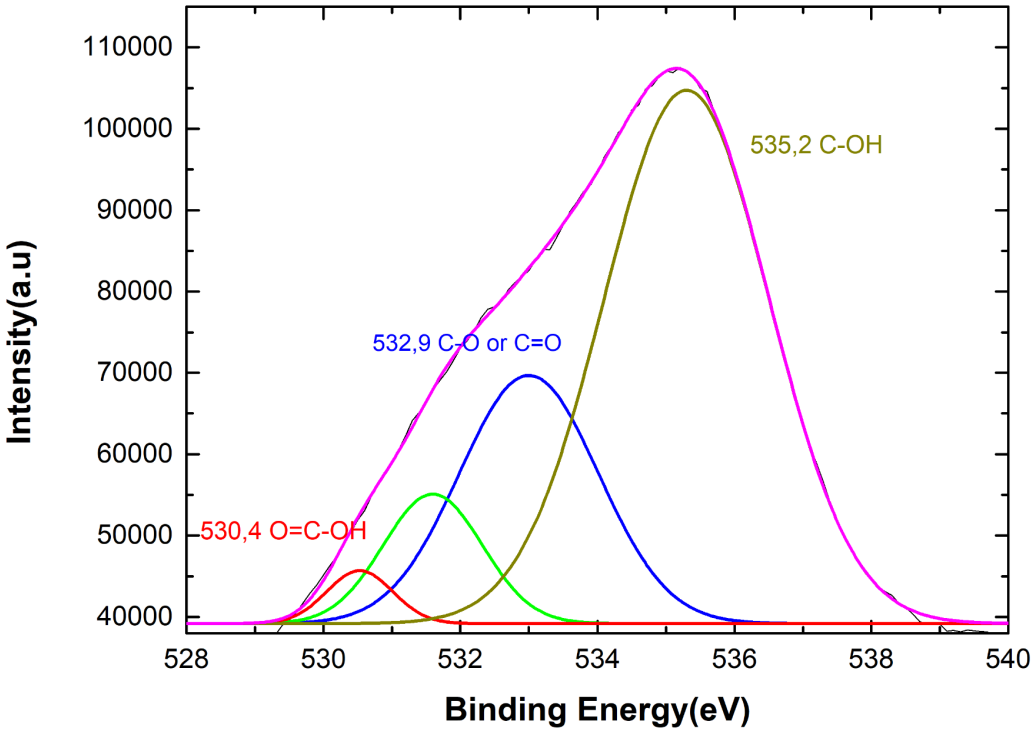


Figure 3.6 *O1s XPS spectra of the sample for 3 min deposition time with 0.25 mA/cm^2 deposition current density.*

In the XPS spectrum, by-products appear, but this was not observed in the Raman Spectroscopy. This is due to the sensitivity of each technique. XPS provides surface elemental and chemical state synthesis of approximately the top 10 nm of the surface of the material. It gives information on the oxidation states of the surface and can identify contaminants. In contrast, Raman spectroscopy provides molecular identification, offering deeper information about the molecular structure and defects present in materials.

3.5 Electrochemical Results

The electrochemical performance of the samples was investigated through the cyclic voltammetry technique, using a three-electrode electrochemical cell. The three electrodes were a graphite foil, a Ag/AgCl and the sample under investigation as the counter, reference and working electrode, respectively. The electrolyte used was 0.1 M Li_2SO_4 and the potential range for the cyclic voltammograms was from -0.7 V to +0.05 V with a scan rate of 30 mV/s. All samples were first scanned and measured at different scanning rates in order to select the

appropriate scan rate. Figure 3.7 shows the cyclic voltammograms of the three samples synthesized with different deposition times, 3, 5 and 10 minutes.

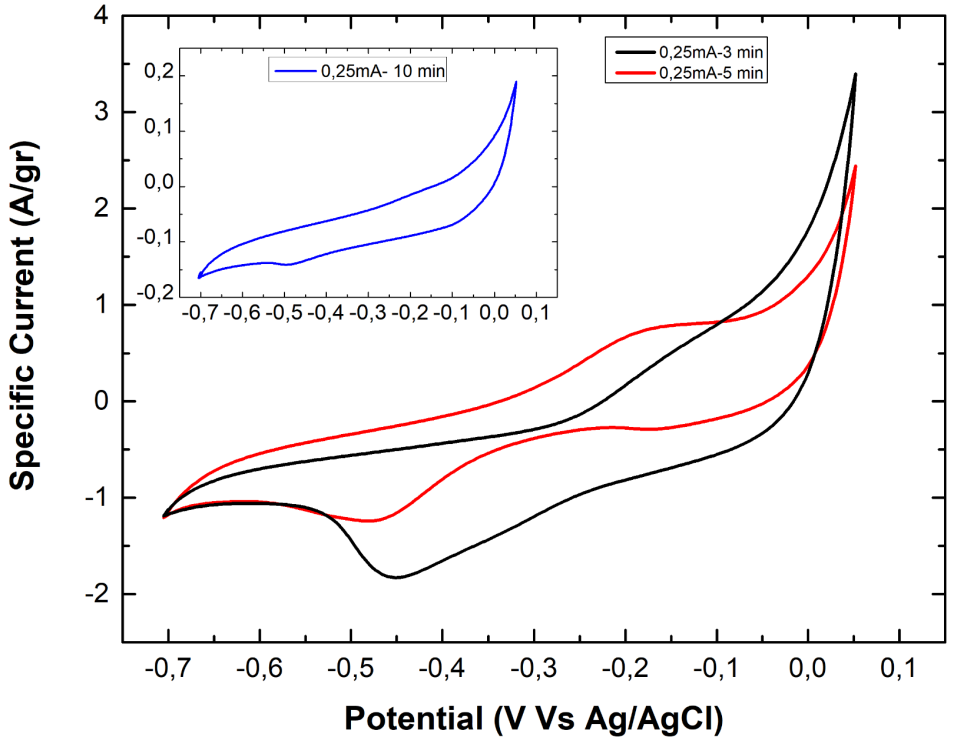


Figure 3.7 *Specific Current-Potential curves of the samples for 3 min (black line), 5 min (red line), 10min (blue line) deposition time with 0.25mA/cm^2 deposition current density with 30mV/s scan rate.*

With respect to the samples with deposition time 3 and 5 min, two anodic peaks are observed at about -0.45 V and at -0.06 V with low intensity as well as one cathode peak at -0.08 V. This fact leads to the conclusion that these redox peaks of the samples do not present reversibility in the Li^+ intercalation/deintercalation process. It is evident that the 5-minute sample exhibits clearer redox peaks, but the area of the curve is comparatively smaller. Moreover, there was a noticeable material removal during the electrochemical measurement, rendering the sample unstable. Conversely, the 10-minute sample does not display visible redox curves. Considering all these factors, it can be concluded that the 3-minute sample shows better electrochemical behavior and stability, thus warranting further investigation into its performance.

The study of the electrochemical behavior of the sample at different scan rates gives important information about the mechanism of intercalation/deintercalation of lithium ions in the lattice of the material. Figures 3.8, 3.9, 3.10 below show the cyclic voltammograms for

the different scan rates ranging from 5 mV/s to 50 mV/s for the electrodeposited GO on Cu keeping the current density constant for 3, 5 and 10 min and the potential range difference from -0,7 V to +0,05 V.

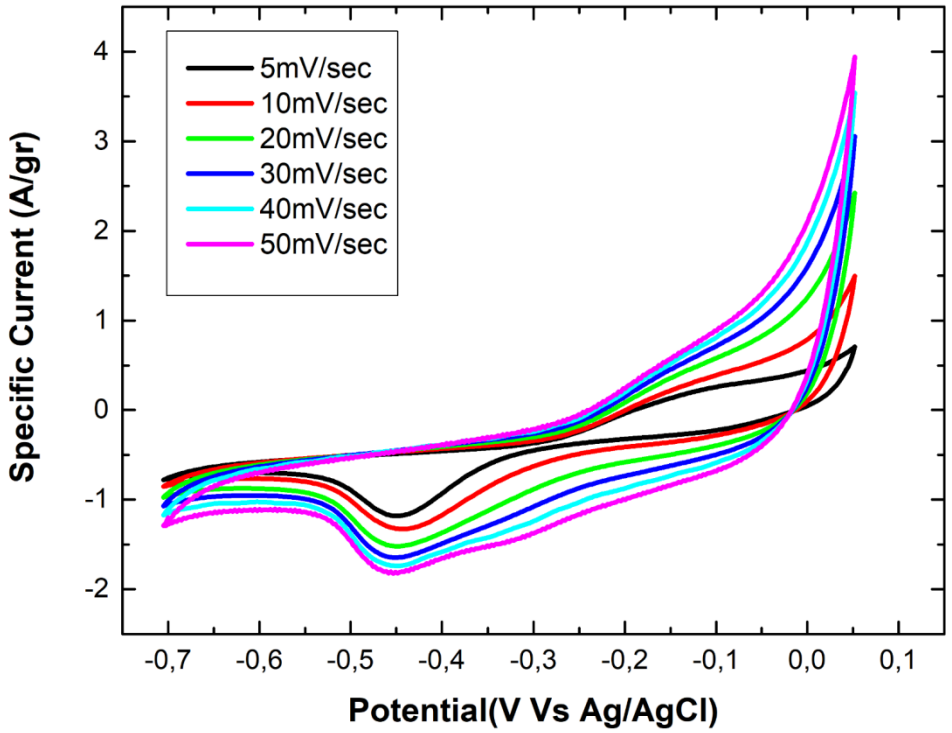


Figure 3.8 *Specific Current*-Potential curves *of 3 min deposition time sample at different scan rates ranging from 5 to 50 mV/s.*

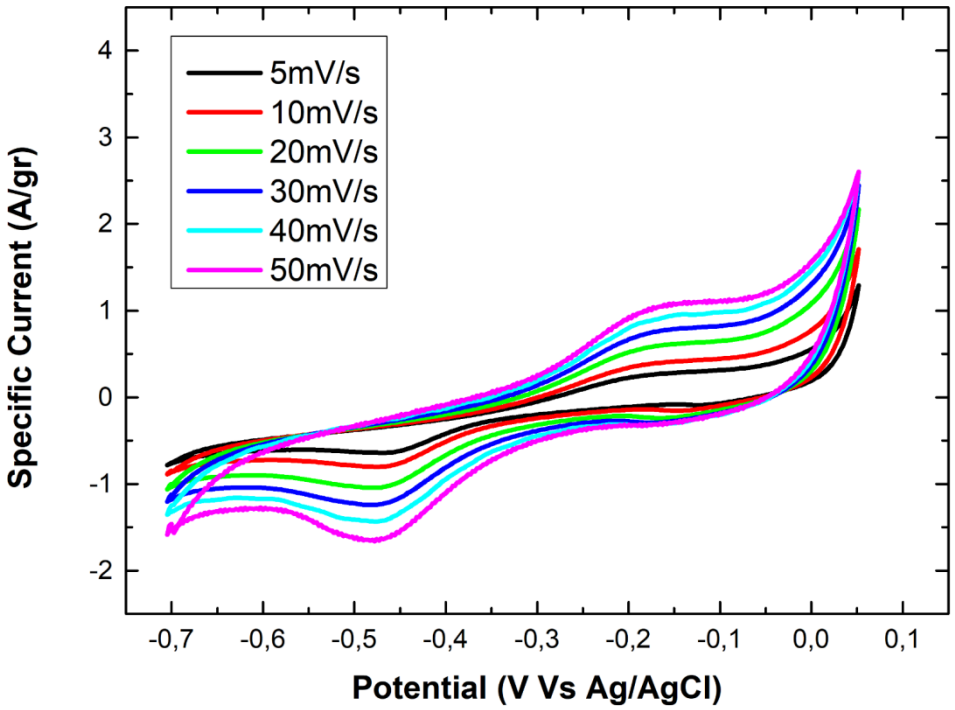


Figure 3.9 *Cyclic voltammograms of 5 min deposition time sample at different scan rates ranging from 5 to 50 mV/s.*

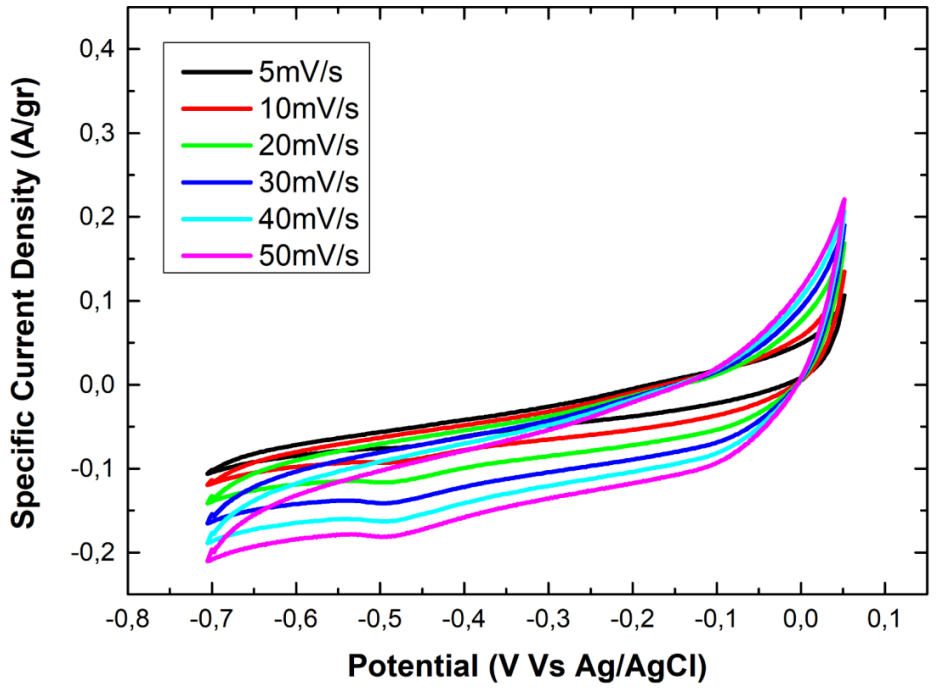


Figure 3.10 *Cyclic voltammograms of 10 min deposition time sample at different scan rates ranging from 5 to 50 mV/s.*

For the sample deposited for 3 minutes, a sharp peak at -0.45 V (anodic) is observed at high scan rates, which seems to shift slightly as the scan rate decreases due to electrochemical polarization. It is worth noting that the electrochemical polarization observed in the cyclic voltammetry plots refers to the changes in current resulting from the redox reactions as the potential is cycled [11]. On the other hand, there appears to be a peak at -0.08 V (cathodic), which remains constant at different scan rates. In the 5-minute sample, these peaks are stronger, with the appearance of an additional peak during the anodic process indicating a non-reversible process. They also seem to shift more strongly with increasing scan rates due to the redox reactions taking place. Finally, the redox peaks are less intense for the 10-minute sample.

The diffusion coefficient is an important parameter that reflects the kinetics of lithium ion intercalation and deintercalation. Based on the literature for the GO, the diffusion coefficient values are in the range of 10^{-10} to 10^{-9} cm^2 s^{-1}, and they show a trend of decreasing as the cell is discharged and charged [12]. Similarly, a study on graphite anodes revealed that the diffusion coefficient with the galvanostatic intermittent titration technique (GITT) ranged from 1×10^{-11} cm^2 s^{-1} to 4×10^{-10} cm^2 s^{-1}. The diffusion coefficient values varied with the specific capacity and lithium concentration, and they tended to increase with increasing lithium concentration. The study emphasized that graphite anodes exhibit sluggish diffusion kinetics for lithium ion intercalation/deintercalation, limiting the rate capability of commercial lithium-ion batteries [13]. In order to calculate the diffusion coefficient, the following formula [14,15,16] was utilized

$$D^{1/2} = \frac{b}{2.72*10^{5} *n^{3/2} *A*C}$$

where,

b is the slope of the graph obtained from the plot of the maximum current of the peaks of the voltammograms for the different scan rates as a function with the square root of each scan rate ($b = \frac{I}{v^{1/2}}$),

n is the charge of ion (Li^+)

A is the area of the electrode (1*1 cm^2)

C is the electrolyte concentration (0.1 M)

To calculate the diffusion coefficient in the 3-min sample, the maximum current was identified in the anodic peak at -0.45 V and in the cathodic peak at -0.08 V from the graphs of the different scan rates (Figure 3.11).

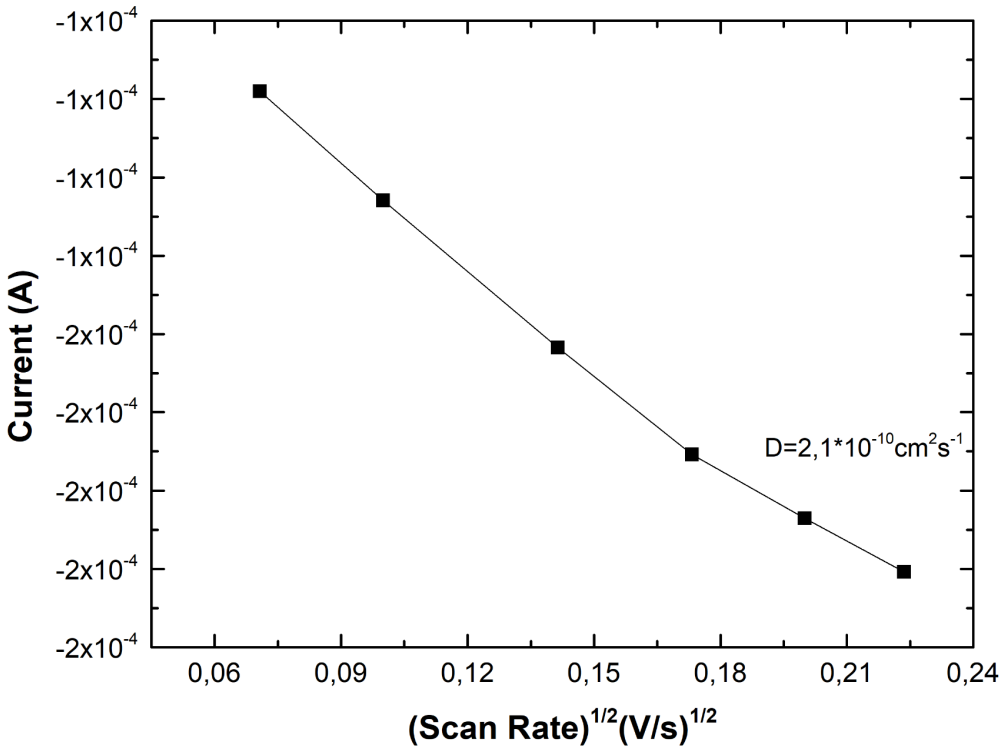


Figure 3.11 *Diffusion Coefficient of the electrodeposited GO for 3 min.*

As shown in Figure 3.11, the sample with a deposition time of 3 minutes exhibits a notably high diffusion coefficient of lithium ions($2.1x10^{-10}$ cm^2 s^{-1}), consistent with findings in literature [14]. This suggests that the rate at which lithium ions traverse the electrode material during charging and discharging is faster. This attribute is particularly critical for high-performance batteries, such as those employed in electric vehicles, which necessitate swift charging and discharging capabilities.

3.5 References

[1] Dubale, Aregahegn A. and Su, Wei-Nien and Tamirat, Gedamu A. and Pan, Chun-Jern and Aragaw, Asefa B. and Chen, Hong-Ming and Chen, Ching-Hsiang and Hwang, Bing-Joe, "The synergetic effect of graphene on Cu2O nanowire arrays as a highly efficient hydrogen evolution photocathode in water splitting",J. Mater. Chem. A",2,43,18383-18397,2014, http://dx.doi.org/10.1039/C4TA03464C

[2] Guide to Evaluating Spectral Resolution on a Dispersive Raman Spectrometer, Thermo Scientific technical note, 2009.

[3] The Importance of Tight Laser Power Control When Working with Carbon Nanomaterials, Thermo Scientific application note, 2010.

[4] Palaniselvam, Thangavelu and Aiyappa, Harshitha Barike and Kurungot, Sreekumar", "An efficient oxygen reduction electrocatalyst from graphene by simultaneously generating pores and nitrogen doped active sites",J. Mater. Chem.",22,45, 23799-23805, 2012,http://dx.doi.org/10.1039/C2JM35128E

[5] Kurniasari et al, "Defect and Magnetic Properties of Reduced Graphene Oxide Prepared from Old Coconut Shell" ,Mater. Sci. Eng., 196, 012021,2017,DOI 10.1088/1757-899X/196/1/012021

[6] Chang, SJ., Hyun, M., Myung, S. et al. "Graphene growth from reduced graphene oxide by chemical vapor deposition: seeded growth accompanied by restoration", Sci Rep 6, 22653,2016, https://doi.org/10.1038/srep22653

[7] Gupta A., Srivastava C.,"Nucleation and growth mechanism of tin electrodeposition on graphene oxide: A kinetic, thermodynamic and microscopic study",Journal of Electroanalytical Chemistry,861, 113964, 2020,https://doi.org/10.1016/j.jelechem.2020.113964

[8] Aliyev E, Filiz V, Khan MM, Lee YJ, Abetz C, Abetz V. "Structural Characterization of Graphene Oxide: Surface Functional Groups and Fractionated Oxidative Debris". Nanomaterials (Basel).18,9,8),1180,doi: 10.3390/nano9081180.

[9] Pooria Moozarm Nia, Hashem Salarzadeh Jenatabadi, Pei Meng Woi, Ebrahim Abouzari-Lotf, Yatimah Alias,"The optimization of effective parameters for electrodeposition

of reduced graphene oxide through Taguchi method to evaluate the charge transfer",Measurement,137,683-690,2019,https://doi.org/10.1016/j.measurement.2019.02.015

[10] Edward P. Randviir,"A cross examination of electron transfer rate constants for carbon screen-printed electrodes using Electrochemical Impedance Spectroscopy and cyclic voltammetry",Electrochimica Acta,286,179-186,2018https://doi.org/10.1016/j.electacta.2018.08.021.

[11] Rui X.H., Yesibolati N., Li S.R. , Yuan C.C. , Chen C.H. , "Determination of the chemical diffusion coefficient of Li+ in intercalation-type Li3V2(PO4)3 anode material",Solid State Ionics,187,1,58-63,2011,https://doi.org/10.1016/j.ssi.2011.02.013

[12] Park JH, Yoon H, Cho Y, Yoo CY. "Investigation of Lithium Ion Diffusion of Graphite Anode by the Galvanostatic Intermittent Titration Technique.", Materials (Basel),14-16,4683 2021,. doi: 10.3390/ma14164683

[13] Zhao Y., Kücher S., Jossen A.,"Investigation of the diffusion phenomena in lithium-ion batteries with distribution of relaxation times",Electrochimica Acta,432,141174,2022,https://doi.org/10.1016/j.electacta.2022.141174.

[14]Bogdan M, Brugger D, Rosenstiel W, Speiser B. "Estimation of diffusion coefficients from voltammetric signals by support vector and gaussian process regression." J Cheminform,28,6:30,May 2014, doi: 10.1186/1758-2946-6-30.

[15] Daskalakis S., Kostopoulou A., Brintakis K., Stratakis E., Prasad Prasadam V., Menguelti K., Bahlawane N., and Vernardou D., " Investigation of Si-Coated Multiwalled Carbon Nanotubes as Potential Electrodes for Multivalent Metal-Ion Electrochemical Energy Storage Systems",The Journal of Physical Chemistry C ,127,27), 13364-13379,2023 ,DOI: 10.1021/acs.jpcc.3c02871

[16] Hsieh, Ming-Chun, Bo-Han Chen, Zhong-Yun Hong, Liu J.K., Pin-Cheng Huang, and Chao-Ming Huang. 2022. "Fabrication of 5 V High-Performance Solid-State Asymmetric Supercapacitor Device Based on MnO_2/Graphene/Ni Electrodes" Catalysts 12, 5, 572,https://doi.org/10.3390/catal12050572

CHAPTER 4-The effect of electrolyte concentration on the electrochemical performance of graphene oxide

After investigating the growth of GO at different deposition times, it was decided to study the effect of electrolyte concentration. This is because elevating the concentration of Li^+ leads to a reduction in the charge transfer resistance.

4.1 Electrochemical Results

Figure 4.1 shows the specific current-potential plots of the three samples examined with different concentrations of lithium sulfate electrolyte.

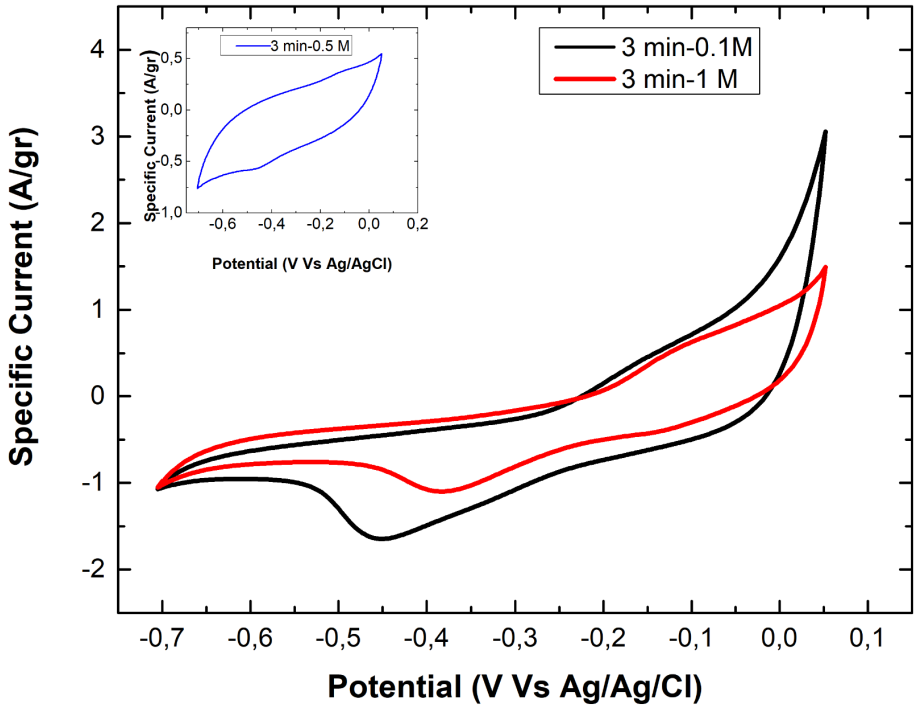


Figure 4.1 *Specific Current-Potential* curves *of the samples for 0.1 M (black line), 1 M (red line) and 0.5 M Li_2SO_4 (blue line) as inset with 3 min deposition time for 0.25mA/cm^2 deposition current density.*

One would expect that with increasing concentration of the electrolyte, the specific current would increase (i.e. more Li^+ for higher electrolyte concentration). However, as observed from the results of cyclic voltammetry, this is not the case. There is probably an inhibition of the intercalation of lithium ions into the graphene oxide lattice due to salt accumulation on

the GO surface for higher concentration. Also, there is a decrease in the redox peaks as the concentration increases and a shift towards the positive values of the potential meaning probably that different processes taking place for the higher electrolyte concentration compared with the 0.1 M.

Figures 4.2, 4.3, 4.4 below show the cyclic voltammograms of the samples with 0.1 M, 1 M and 0.5 M of Li_2SO_4 for 3 min deposition time and 0.25 mA/cm^2 current density, respectively at different scan rates ranging from 5 mV/s to 50 mV/s.

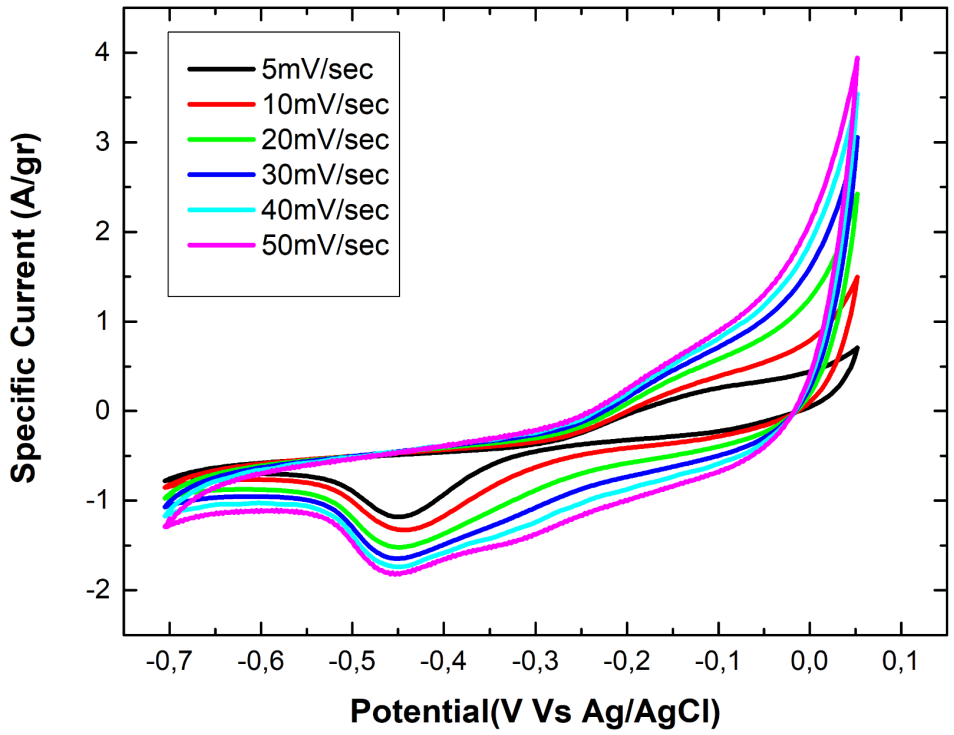


Figure 4.2 *Specific Current-Potential graphs of 3-min GO electrodeposited sample in 0.1 M Li_2SO_4 at different scan rates.*

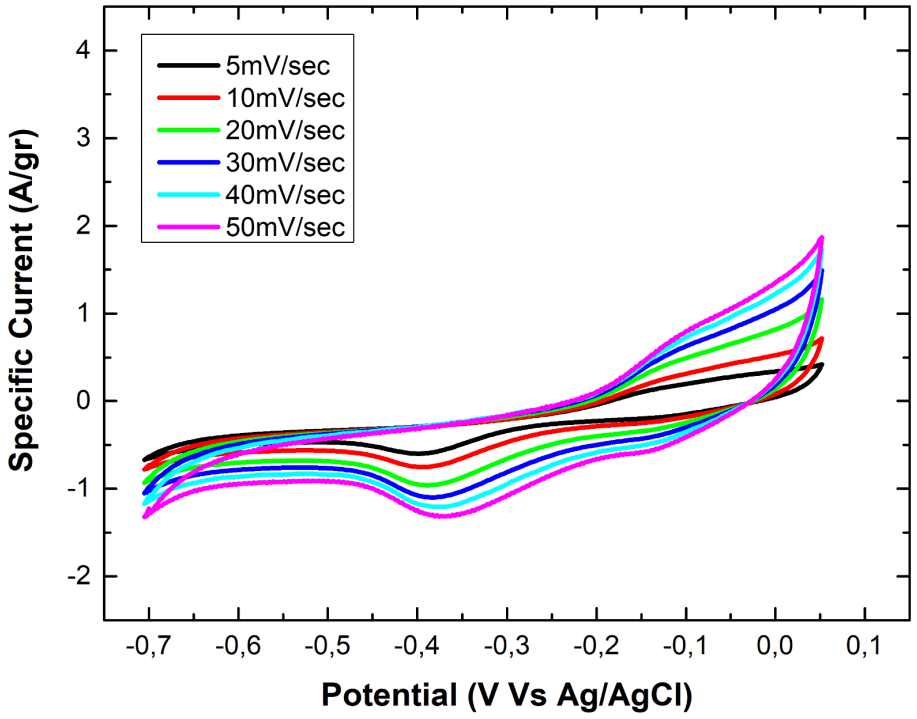


Figure 4.3 *Specific Current-Potential graphs of 3-min GO electrodeposited sample in 1 M Li_2SO_4 at different scan rates.*

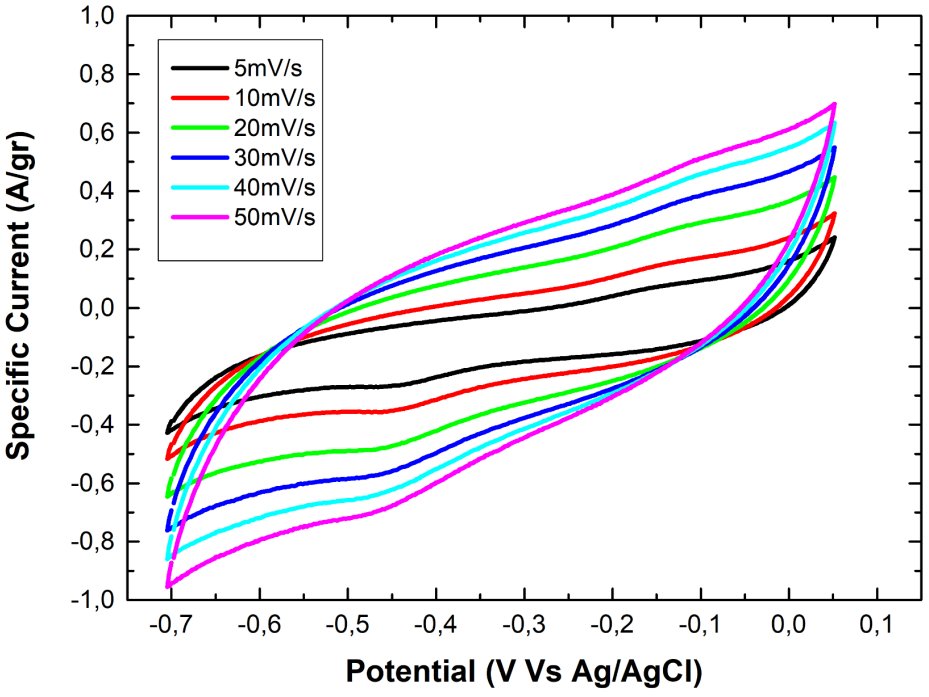


Figure 4.4 *Specific Current-Potential graphs of 3-min GO electrodeposited sample in 0.5 M Li_2SO_4 at different scan rates.*

From the curves of different scan rates, similar behavior is observed in the samples with 0.1 M and 1 M electrolyte concentration (i.e. they show two anodic and one cathodic peak), with the 0.1 M concentration exceeding specific current (higher current values and larger curve area). The sample with the lowest electrolyte concentration (0.1 M) shows a sharp peak at -0.45 V (anodic) at high scan rates, which appears to shift slightly as the scan rate decreases; also, there appears to be a peak at -0.08 V (cathodic) which remains constant at different scan rates. In the sample with the highest electrolyte concentration, the corresponding peaks appear to be shifted to the positive direction at -0.37 (anodic), while the second peak in the cathode remains at the same position (-0.08 V). These are more intense but appear to shift more strongly with increasing scan rates, probably due to a more powerful electrochemical polarization. Interestingly, the sample with an electrolyte concentration of 0.5 M seems to behave more like a capacitor as it does not show redox peaks. This may be due to a change in the structure of GO due to the repeated use of the dispersion in electrodeposition processes of particular series. This aspect warrants further exploration in future research endeavors.

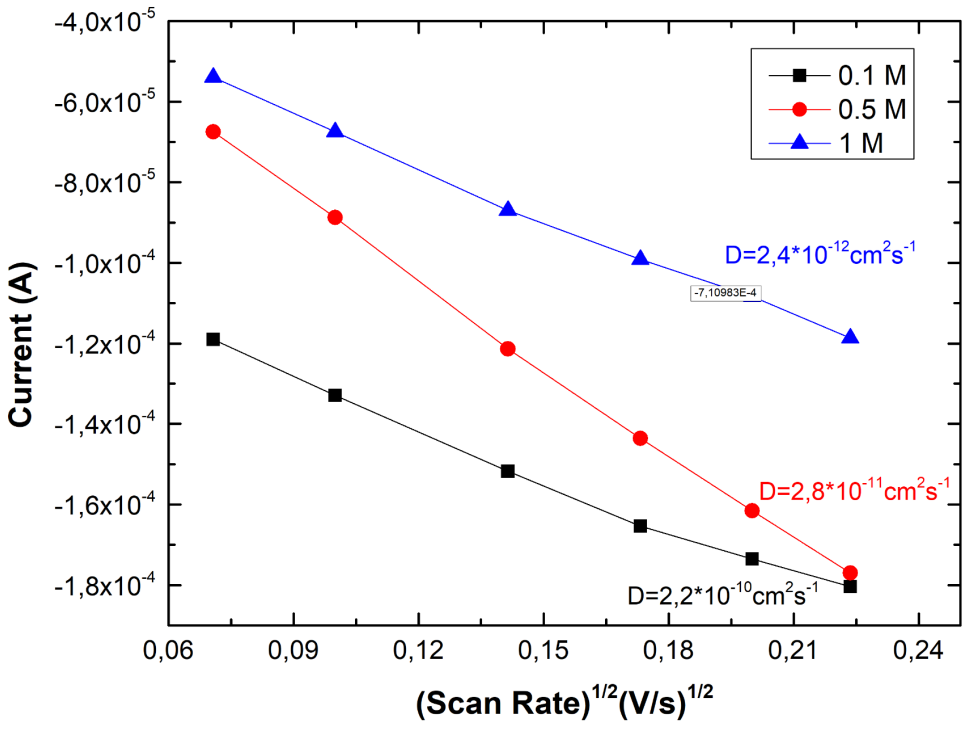


Figure 4.5 *Diffusion coefficient of electrodeposited GO samples studied in 0.1 M (black line), 0.5 M (red line), 1 M Li_2SO_4 (blue line).*

From the graph of the diffusion coefficient (Fig 4.5), one can see that in the sample with the lowest electrolyte concentration, the diffusion coefficient of lithium-ion is higher than in the sample with the highest electrolyte concentration. This is also consistent with cyclic voltammetry curves. It is therefore verified that when the concentration of the electrolyte increases, lithium ions probably have difficulty intercalating into the lattice of the material.

From the results of the electrochemical measurements, it appears that the sample with the lowest electrolyte concentration shows better electrochemical behavior with faster diffusion of electrolyte ions in the lattice of the material. For all of the above, it is worth further investigating the stability of the samples in a continuous cycle of intercalation and deintercalation. In the following section, the stability of samples with the best results obtained for electrolyte concentration of 0.1 M and 1 M are investigated and compared, in order to further understand and evaluate the electrochemical behavior of the two samples.

4.2 Stability of the GO in different electrolyte concentrations

4.2.1 Electrochemical Results

Another parameter that needs to be investigated is the stability of the buffer layer. For its evaluation, the electrodeposited GO was continuously cycled for 1, 250 and 600 in 0.1 and 1 M Li_2SO_4 (Figures 4.6, 4.7).

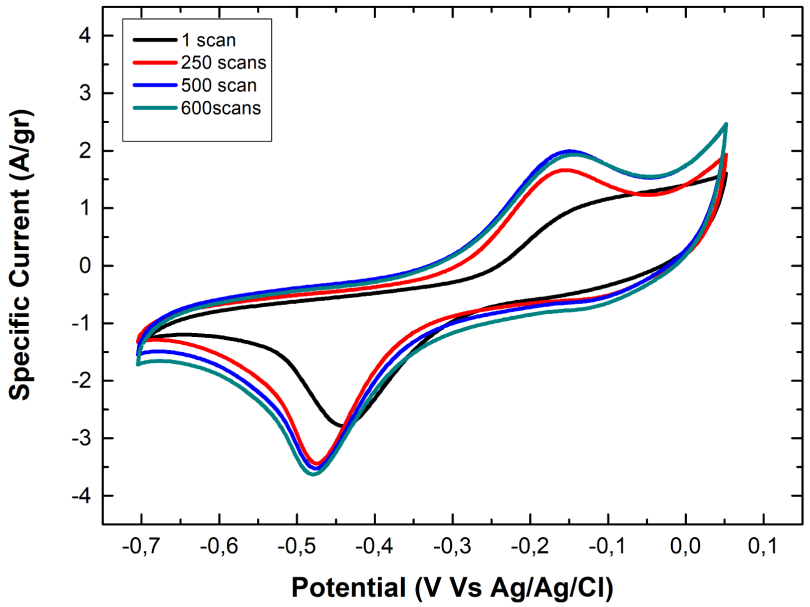


Figure 4.6 *Specific Current-Potential graphs of electrodeposited GO samples studied in 0.1 M Li_2SO_4 for 1, 250, 500 and 600 scans.*

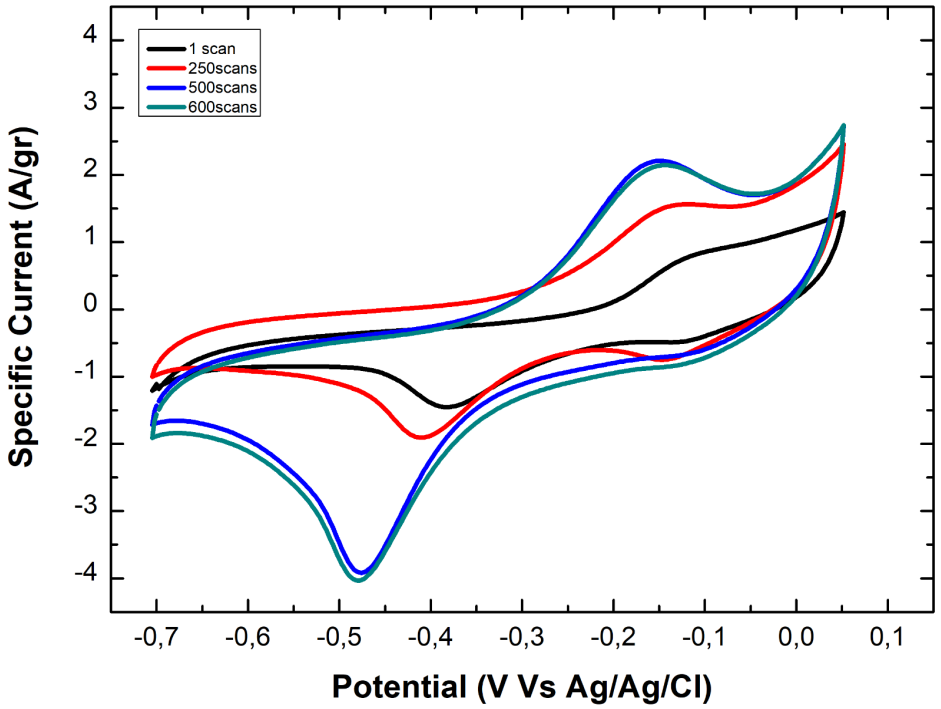


Figure 4.7 *Specific Current-Potential graphs of electrodeposited GO samples studied in 1 M Li_2SO_4 for 1, 250, 500 and 600 scans.*

Cyclic voltammetry diagrams show similar behavior in both samples. Two anodic peaks are observed at about -0.45 V and at -0.06 V, as well as a cathode peak at -0.08 V (thus, the intercalation/deintercalation of Li^+ process is not reversible). It is worth noting that with the increase in scans, the specific current also increases up to 250 scans with the redox peaks appearing at various positions. Subsequently, the specific current remains constant after 250 scans (i.e. superposition of the curves), likely due to the material undergoing a structural change from the 1st to the 250th scan. After the 600 intercalation/deintercalation scans, a decrease in specific current was observed due to sample deterioration as observed in the transparent electrochemical cell.

4.2.2 SEM/EDS Results

The samples were investigated before and after the 600 scans with SEM/EDS to study whether there was a change in their morphology. SEM/EDS analysis after 600 scans (Table 4.1 and Figures 4.8,4.9,4.10), shows that the elemental composition is altered due to possible exfoliation of the material layers (the amount of oxygen is increased after cyclic

voltammetry).This is due to the fact that the interference of the aqueous electrolyte anions is facilitated by the simultaneous formation of root species (e.g. OH and O) from the oxidation of water (at about +1V). These radical species oxidize/break down the graphite structure starting from the edges and result in an increase in the openings available for anions to penetrate, as reported in a study by Adriano Ambrosi et al. [1]

Element	Before CV at%	After CV at% (0,1 M)	After CV at% (1 M)
C	51	41	34
O	40	52	56
S	0,44	1,92	2,96
Cu	7,91	3,37	6,82

Table 4.1 *The at. % of elements before and after CV of the electrodeposited GO studied in 0,1 and 1 M Li_2SO_4 electrolyte.*

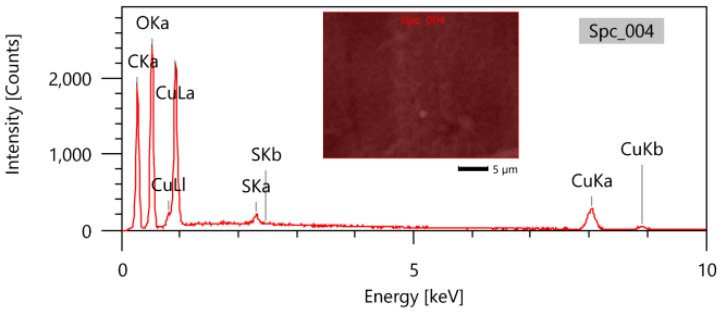


Figure 4.8 *Elemental mapping and EDS of the electrodeposited GO studied in 0.1M Li_2SO_4 electrolyte before CV*

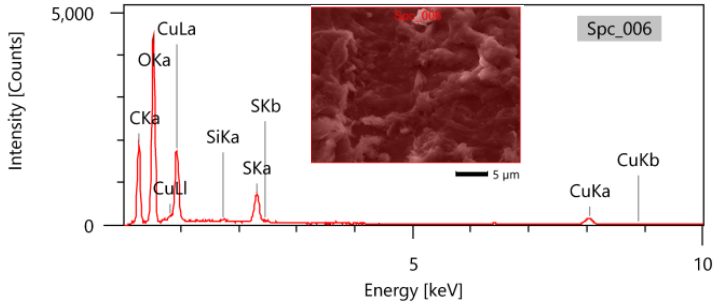


Figure 4.9 *Elemental mapping and EDS of the electrodeposited GO studied in 1 M Li_2SO_4 electrolyte after CV*

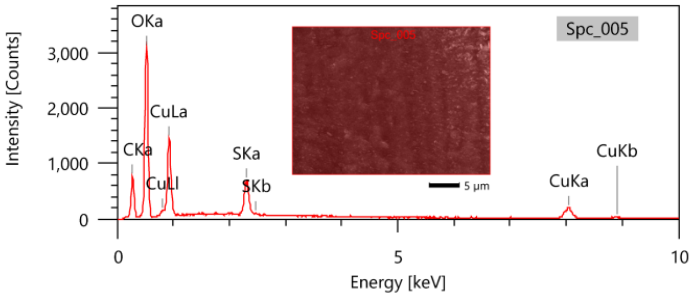


Figure 4.10 *Elemental mapping and EDS of the electrodeposited GO studied in 0.1M Li_2SO_4 electrolyte after CV*

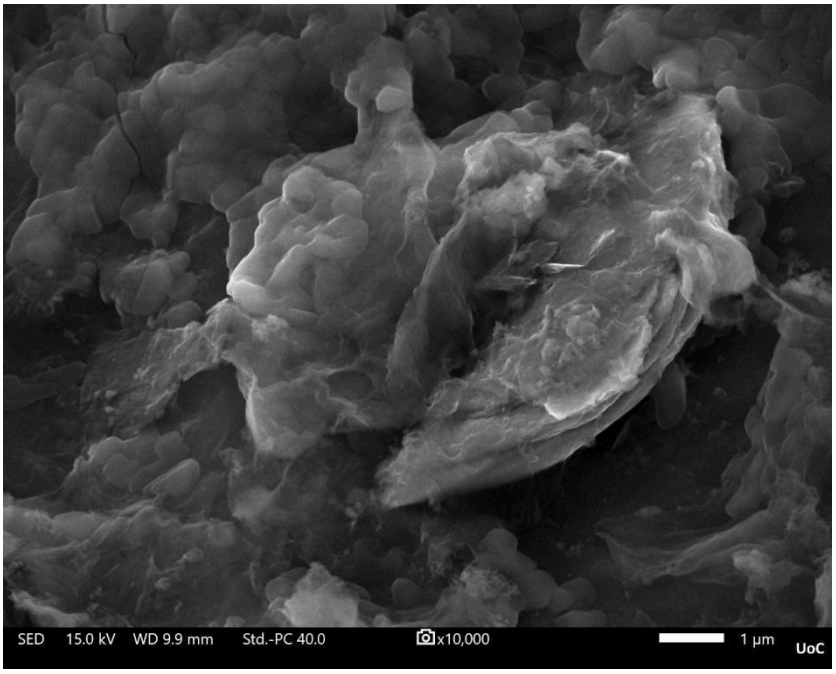


Figure 4.11 *SEM images of the electrodeposited GO studied in 0.1M Li_2SO_4 electrolyte after CV*

As shown in Figure 4.11, the morphology of the sample after the cyclic voltammetry measurements has changed. The continuous intercalation and deintercalation cycles appear to have caused aggregates on the surface of the GO. Additionally, one could notice by looking Figure 4.12 that the morphology of the electrodeposited GO sample studied in 1 M electrolyte concentration differs from the one with the lowest electrolyte concentration. Flake-like surfaces are in relation to the structure at the lowest concentration, due to the possible exfoliation of the material as mentioned above. This explains the fact that the material showed cracks after the scans were completed, as could be observed from the transparent electrochemical cell.

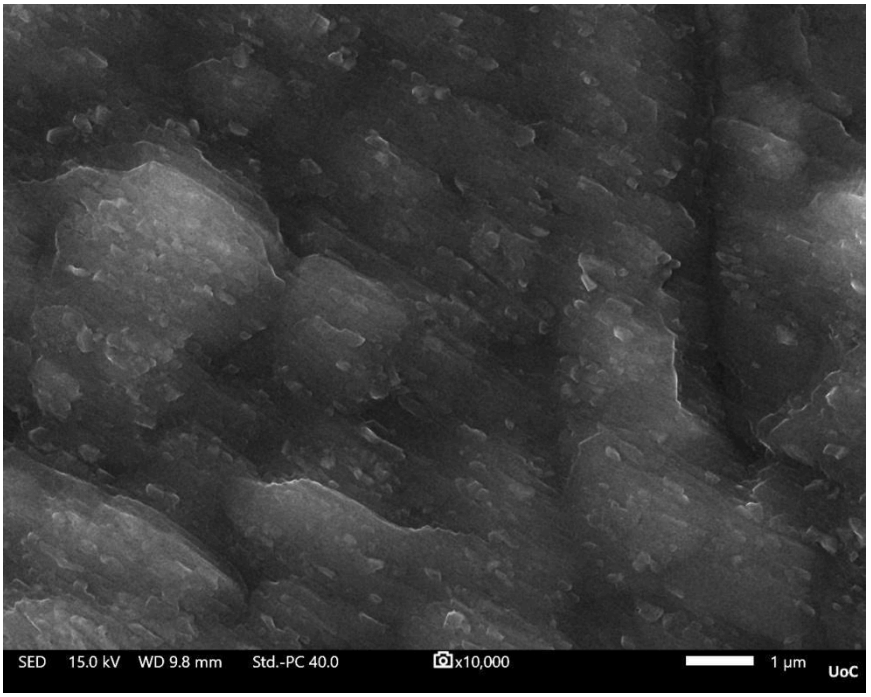


Figure 4.12 *SEM images of the electrodeposited GO studied in 1M Li_2SO_4 electrolyte after CV*

4.2.3 XPS Results

To fully investigate if the samples have undergone structural alterations after the 600th scan, XPS measurements were performed. From the XPS spectra, the initial hypothesis is verified that after 600 intercalation/deintercalation scans, the structure of the material has been altered. As shown in Figure 4.13, the peaks around ~284.6 eV are attributed to the C-C and C=C lattices of graphene. The epoxy and phenolic -OH-bonded carbons show relative binding energy at ~286.6 eV, while the corresponding signals of ketone, lactone and carboxyl-containing carbons are at ~288,5 eV. Taking into consideration Figure 3.6, the carbon element is different after cyclic voltammetry. More specifically, the peaks of the ketone and quinone groups for the 0.1 M sample are shifted to the left (~286.6 eV) compared to the same sample before recycling (~290.3 eV). A similar change is observed in the 1 M sample in which the peak of the ketone groups is shifted flatter and lower in intensity (287.7 eV). This is probably due to the exfoliation of the material planes as suggested by Adriano Ambrosi et al. in their study, the change in the sign of quinone-hydroquinone pairs in the XPS spectrum is due to exfoliation of the graphene oxide planes.Furthermore, it appears that the intensity of the D band of graphene oxide appears to have increased after cyclic voltammetry.

This structural change also appears morphologically through the SEM images, as described in the previous section.

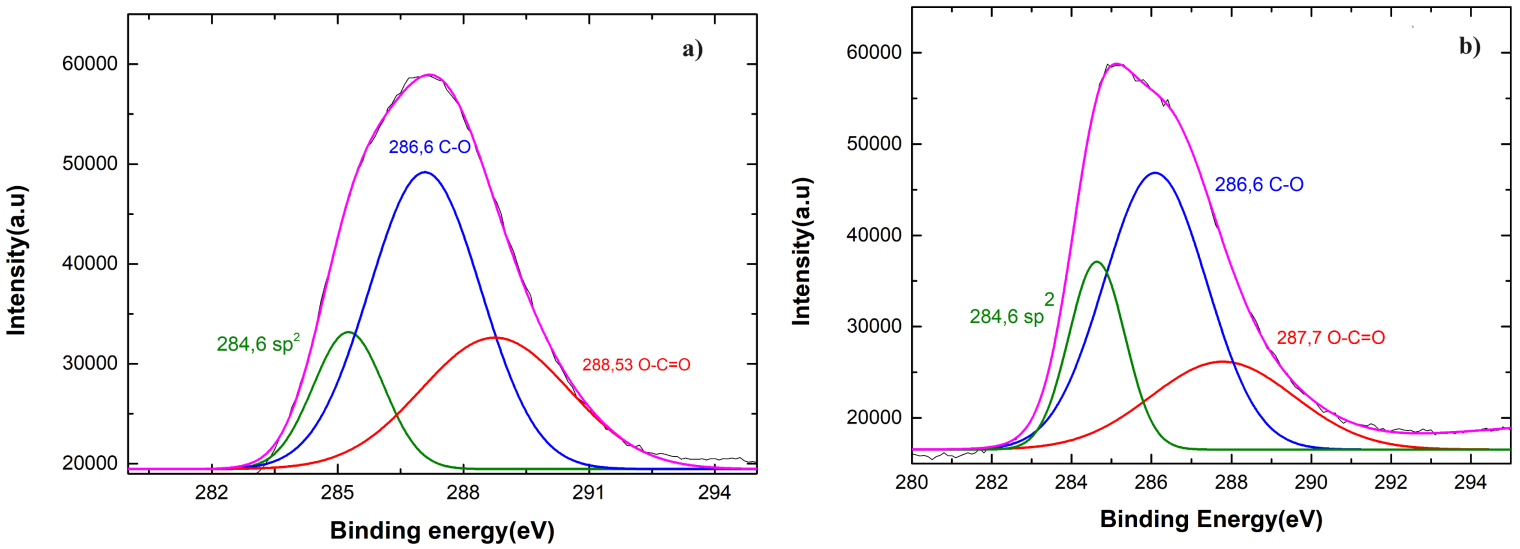


Figure 4.13 *C1s XPS spectra after CV of the electrodeposited GO sample studied in a) 0.1 M* Li_2SO_4 and b) *1 M* Li_2SO_4.

The results from O1s spectra of GO samples confirm the C1s results according to which the graphite structure is strongly oxidized and contains different oxygen functionalities. Therefore, the signal around ~530 eV corresponds to the bonds O=C-OH, ~532 eV attributes to C-O and O–C=O from carboxylic group and the signal around ~535,2 eV corresponds to phenolic –OH and epoxy groups

From the XPS spectra of the oxygen element (Figure 4.14), in the 0.1 M sample there is a shift in the peak of the phenolic-OH and epoxy groups (~534.2), while in the higher concentration sample there is a significant decrease in the intensity of the C-OH bond (~50000 a.u intensity compared to the sample before the cyclic voltammetry which was ~100000 a.u), which confirms that the graphene oxide layers have probably been exfoliated and electrolyte ions have intercalated them.

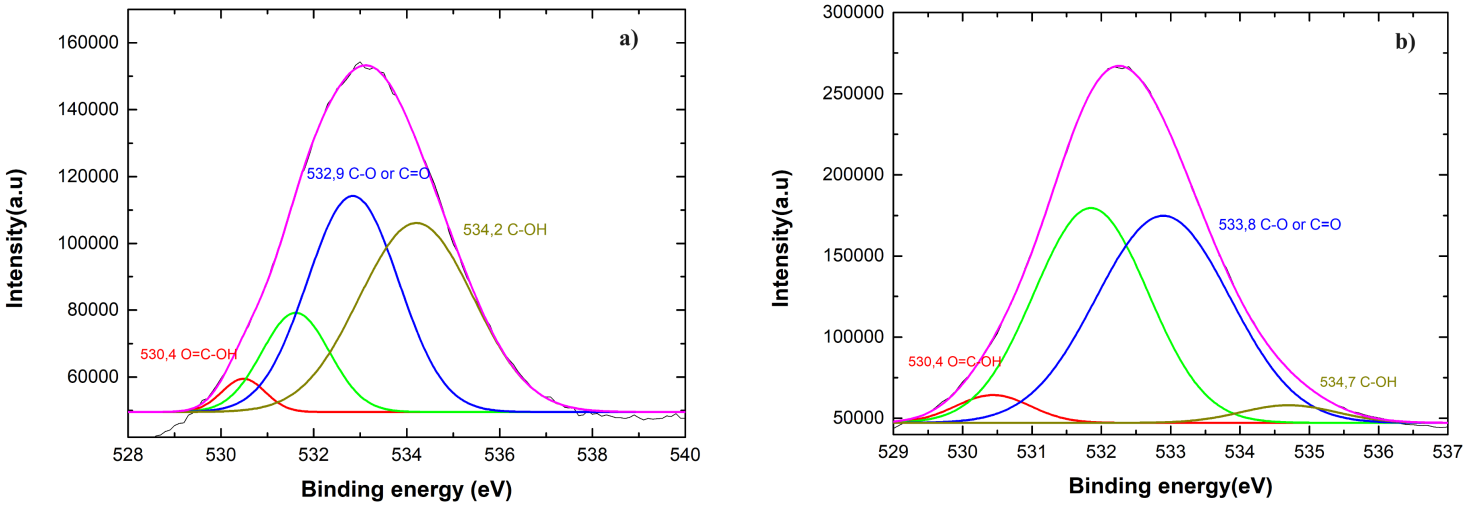


Figure 4.14 *O1s spectra after CV of the electrodeposited GO samples studied in a) 0.1 M Li_2SO_4 and b) 1 M Li_2SO_4.*

According to all the above, we conclude that the sample with 3-minute deposition and electrolyte concentration of 0.1 M, shows better stability. This is also verified through structural and morphological measurements since it does not appear to have suffered any particular deterioration after 600 scans.

4.3 References

[1] Ambrosi A., Kiang C.C., Naziah M. L., Huiling Loo A., Hong An Wong C., Yong Sheng Eng A.,Bonanni A. and Pumera M.,"Graphene and its electrochemistry – an update",Chem.Soc.Rev.,45,9,2371–2716,2458 7 May, 2016 , 2016, https://doi.org/10.1039/C6CS00136J.

CHAPTER 5. Effect of graphene oxide ratio on the electrochemical performance of graphene oxide

After investigating the growth of GO at different deposition times and the effect of electrolyte concentration, it was decided to study the effect of the GO:H_2O dispersion ratio, expecting that a higher amount of GO would increase the electrical conductivity and the performance of the materials. The solution prepared in this set of experiments had a ratio of 3:1 GO:H_2O. The electrodeposition of GO on a Cu substrate was performed for 3 minutes with a deposition current density of 0.25 mA/cm^2, as this sample showed better results.

5.1 SEM Results

Figure 5.1 shows the SEM images of the samples with GO:H2O ratios of 2:1 and 3:1, respectively for 3 minutes deposition time with 0.25 mA/cm^2 deposition current density. The sample with a ratio of 3:1 shows to form clusters probably due to the higher amount of material deposited in the substrate. On the contrary, the thickness of the two samples (Figure 5.2) does not show any differences leading to the conclusion that the deposited material is not related to the amount of GO in the dispersed solution.

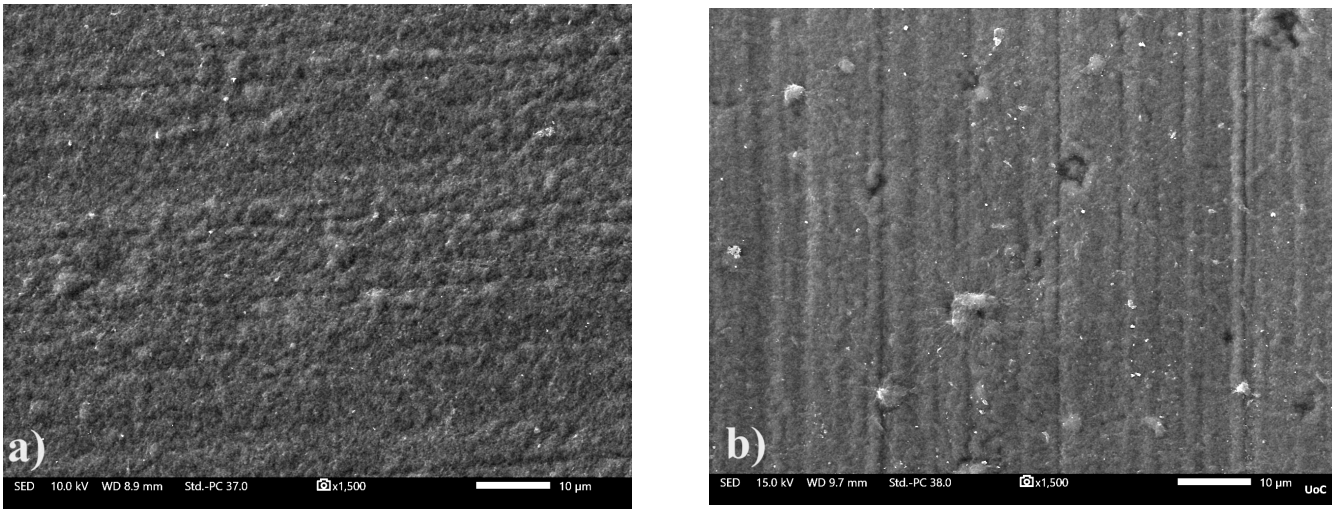


Figure 5.1 *SEM images of a) 2:1 GO:H_2O ratio and b) 3:1 GO:H_2O ratio at 3 min deposition time with 0.25 mA/cm^2 deposition current density.*

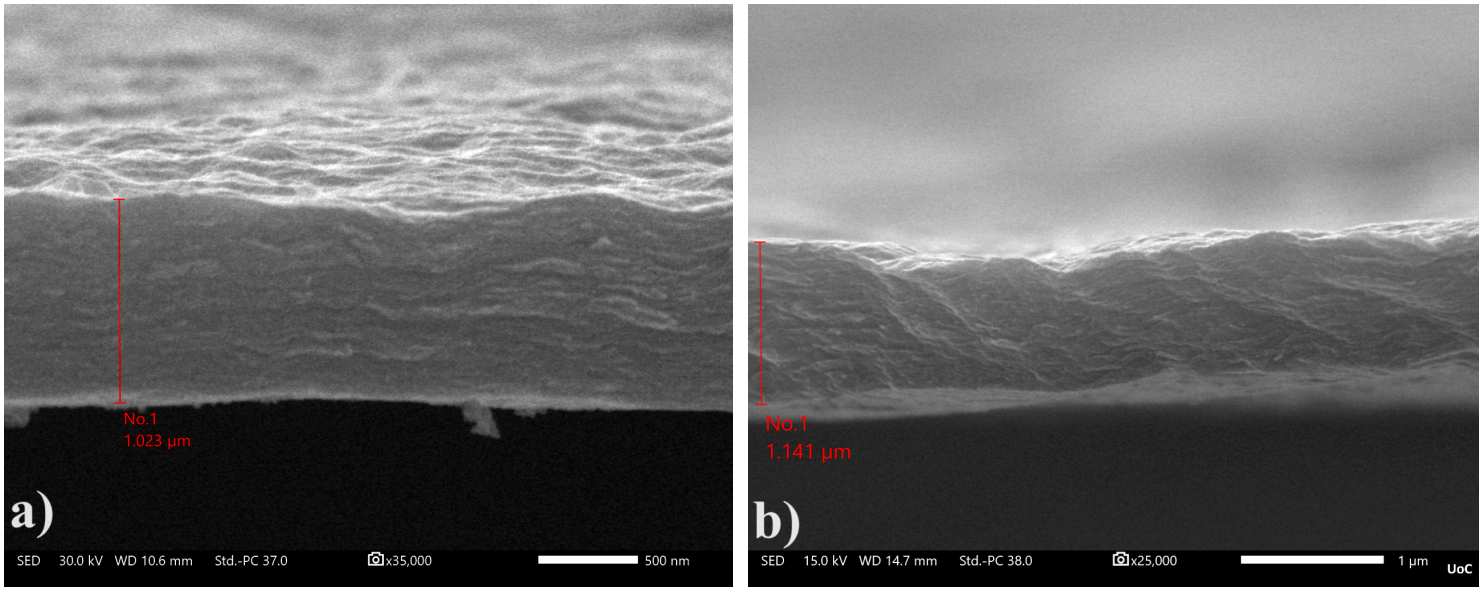


Figure 5.2 *SEM images of a) 2:1 GO:H_2O ratio b) 3:1 GO:H_2O ratio at 3 min deposition time with 0.25 mA/cm^2 deposition current density.*

5.2 Electrochemical Results

Figure 5.3 shows the Specific Current-Potential plots of the two samples synthesized with different GO:H_2O ratios.

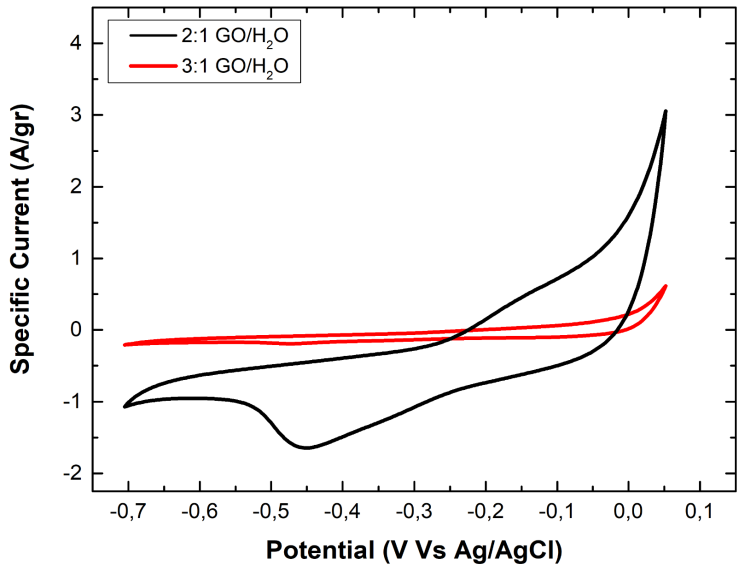


Figure 5.3 *Specific Current-Potential graphs of samples 2:1 GO:H_2O and 3:1 GO:H_2O ratio studied in 0.1 M of Li_2SO_4 electrolyte.*

One would expect that by increasing the proportion of GO in the dispersing aqueous solution, the specific current would increase or at least be of the same order of magnitude as that of the lower ratio. However, as observed from the results of cyclic voltammetry, this does not occur. It is possible that the increase in the amount of GO prevents the homogenisation of the dispersion solution. Possibly, i.e. the problem occurs at the initial step of the dispersion synthesis and its homogenisation via ultrasonic probe and for this reason it shows these electrochemical results. Furthermore, it is important to mention that during the immersion of the electrodeposited GO (higher ratio GO:H_2O) in the electrolyte for electrochemical measurements, a portion of the deposit was detached from the substrate. This could explain the lower specific current observed in CV, leading to the inference that the sample is not stable.

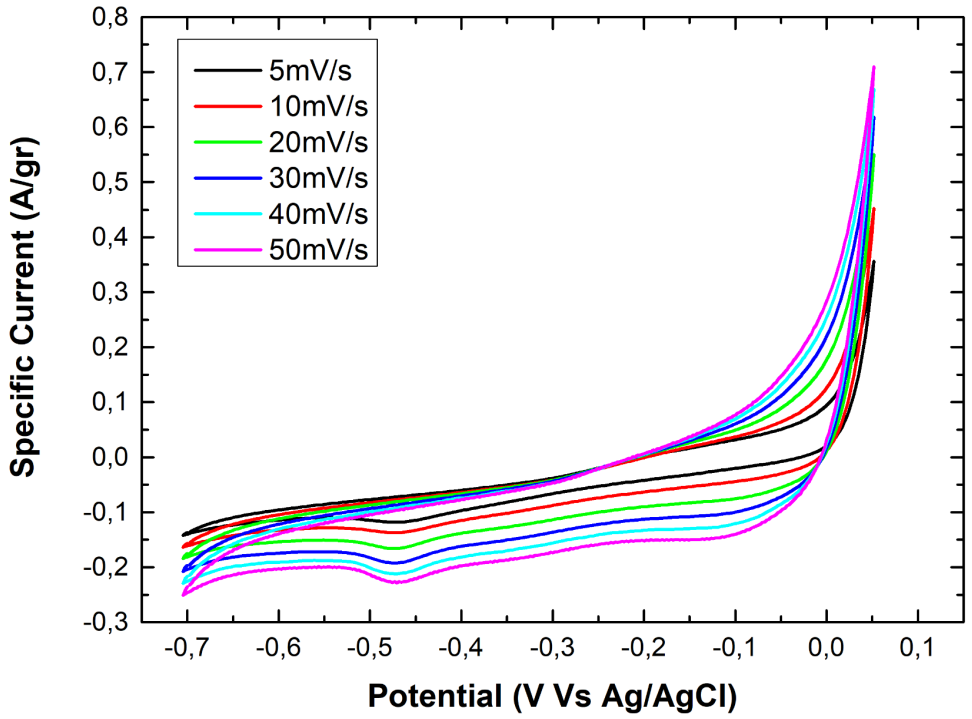


Figure 5.4 *Specific Current-Potential* curves *of 3:1 GO:H_2O ratio sample studied in 0.1 M of Li_2SO_4 electrolyte at different scan rates ranging from 5 to 50 mV/s.*

Concerning the various scan rates (Figure 5.4), there appears to be consistency, although clear redox peaks are absent. This is likely due to the sample's damage from the removal of the deposit, as previously mentioned. It is noteworthy that the diffusion coefficient in the sample

with the highest GO ratio could not be calculated due to the lack of distinct redox peaks in the CV graphs at different scan rates.

.

CHAPTER 6. Effect of deposition current density on the electrochemical performance of graphene oxide

In an effort to increase the effective surface area of the synthetic electrodes, the sample with a deposition time of 5 minutes was selected to improve its stability and study the growth mechanism at higher deposition current densities of 0.25, 0.5 and 0.75 mA/cm^2. The characterization measurements performed were Raman spectroscopy to confirm the presence of graphene oxide, SEM to obtain information about the morphology of the samples and their thickness to estimate the growth mechanism, and CV to study their electrochemical behavior and stability in continuous cycles of interference and interference.

6.1 Raman Spectroscopy Results

From Figure 6.1, one observes that the band D is slightly offset (about 1355 cm^{-1}) compared to the theoretical value (~1350 cm^{-1}). Correspondingly, a similar displacement occurs in the band G, which is approximately 1387 cm^{-1} relative to the theoretical value (~1590 cm^{-1}) [1]. This behavior justifies that in graphene oxides, the D band could be related with disorder graphitic lattice due to the presence of C sp^3 bonds. For all the above, the sample with current density of 0.25 mA/cm^2 (black line) for a deposition time of 5 minutes appears to have better crystallinity than the other two with 0.5 mA/cm^2 (red line) and 0.75 mA/cm^2 (blue line), due to the fact that the peak intensities are higher and the peak widths are narrower.

Moreover, in the Raman spectrum, the ratio of ID/IG intensities (Fig. 6.2) in all three samples is close to 1, suggesting that the degree of disorder of the structure of the prepared graphene is relatively low.

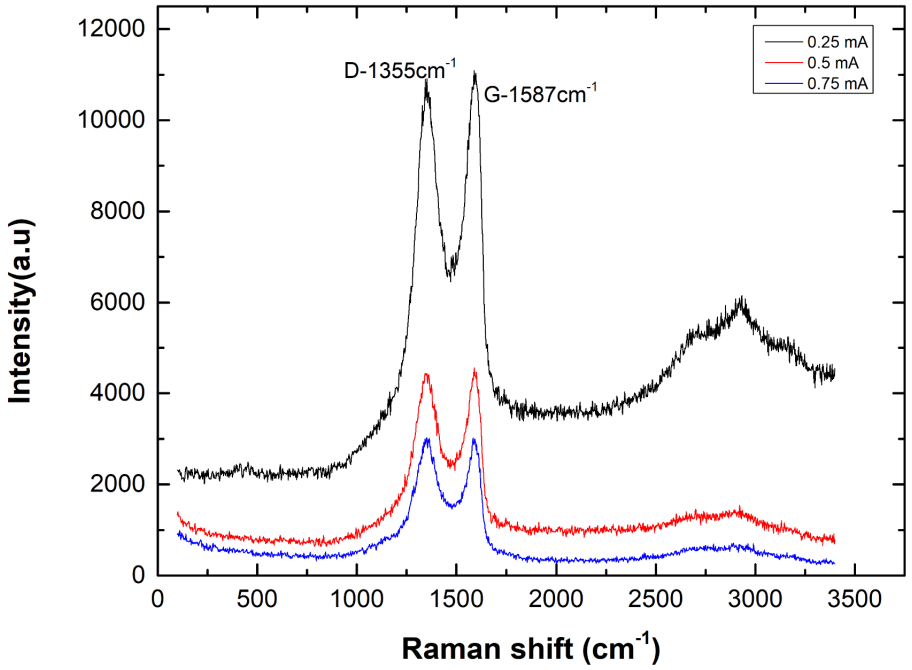


Figure 6.1 *Raman spectra of synthesized samples with a constant deposition time 5 min and deposition current densities, 0.25 mA/cm^2 (black line), 0.5 mA/cm^2 (red line) and 0.75 mA/cm^2 (blue line).*

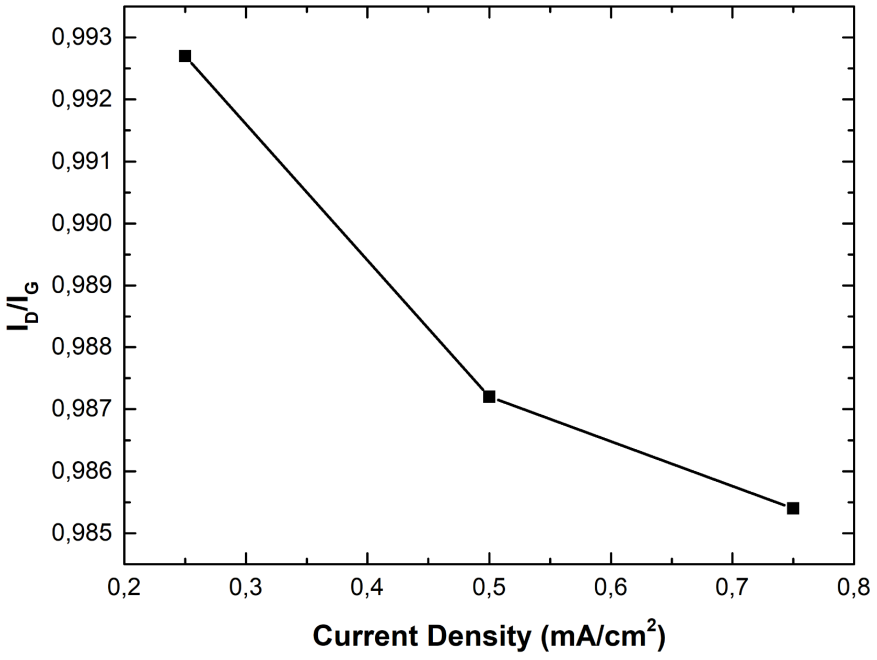


Figure 6.2 *The diagram of the I_D/I_G ratio as a function with the different deposition current densities.*

6.2 SEM Results

Figure 6.3 shows SEM images of GO samples with different deposition current densities (i.e. 0.25, 0.5 and 0.75 mA/cm^2). It can be observed that there is a difference in the morphology of the three samples. As the deposition current density increases, aggregates are formed on the surface of the substrate with a decrease in the thickness of the deposit. (Figure 6.4 and Table 6.1). These aggregates probably affect the adhesion of GO on Cu substrate, causing cracking which was also observed visually (the deposit was removed very easily).

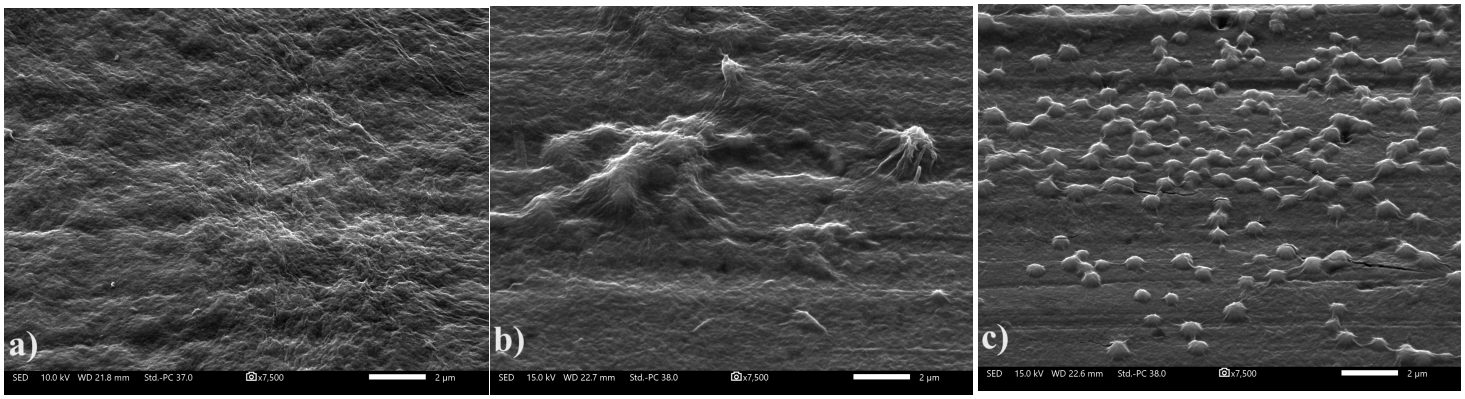


Figure 6.3 *SEM images of GO samples with a)* 0.25 mA/cm^2, *b)* 0.5 mA/cm^2 *and c)* 0.75 mA/cm^2 *deposition current densities on Cu substrate with 5 min deposition time. The magnification in all images is x7,500 and the line is equal to 2 µm.*

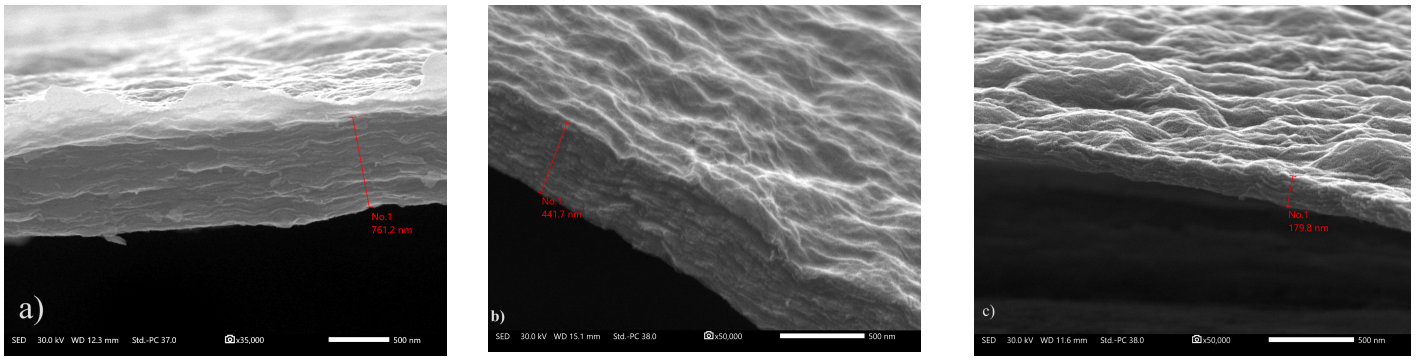


Figure 6.4 *The cross-section SEM analysis of a)* 0.25 mA/cm^2 *b)* 0.5 mA/cm^2 *and c)* 0.75 *mA*/cm^2 *deposition current density for 5 min deposition time. The magnification in a,b and c images is x 50,000 and the line is equal to 500 nm.*

Deposition current density	Thickness (nm)
0.25 mA/cm^2	761,2
0.5 mA/cm^2	441,7
0.75 mA/cm^2	179,8

Table 6.1. The thicknesses of electrodeposited GO for 5 minutes with 0.25 mA/cm^2 0.5 mA/cm^2 and 0.75 mA/cm^2 current density.

6.3 Electrochemical Results

The electrochemical performance of the samples was investigated through the cyclic voltammetry technique, using 0.1 M Li_2SO_4 and the potential range from -0.7 V to +0.05 V with a scan rate of 30 mV/s (Figure 6.5).

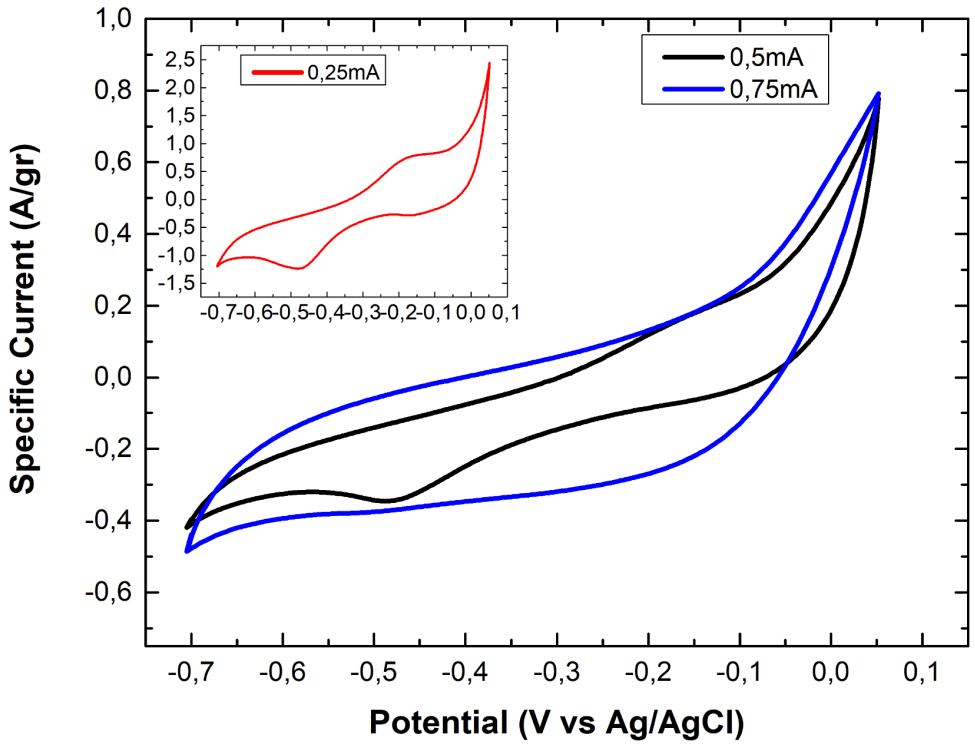


Figure 6.5 *Specific Current-Potential curves of the GO electrodeposited samples with 0.25 mA/cm² (red line) 0.5 mA/cm² (black line), 0.75 mA/cm² (blue line) deposition current density for 5 min deposition time.*

Electrodeposited GO for 0.5 mA/cm² and 0.75 mA/cm² exhibit a lower specific current, as indicated by a smaller area under the curve, compared to the sample with the lowest deposition current density of 0.25 mA/cm². Additionally, it is apparent that the sample for a deposition current density of 0.75 mA/cm² displays a distinct curve and lacks observable redox peaks in contrast to the other two. Importantly, even in samples subjected to higher current densities, the deposited material was removed upon immersion in the electrolyte, indicating their instability. This is also evident from Raman spectra of the samples in which their peak intensities are significantly lower for the highest current density. To get a more complete view of the effect of current density on the GO growth mechanism and properties, it would be useful to make XPS measurements in possible future work.

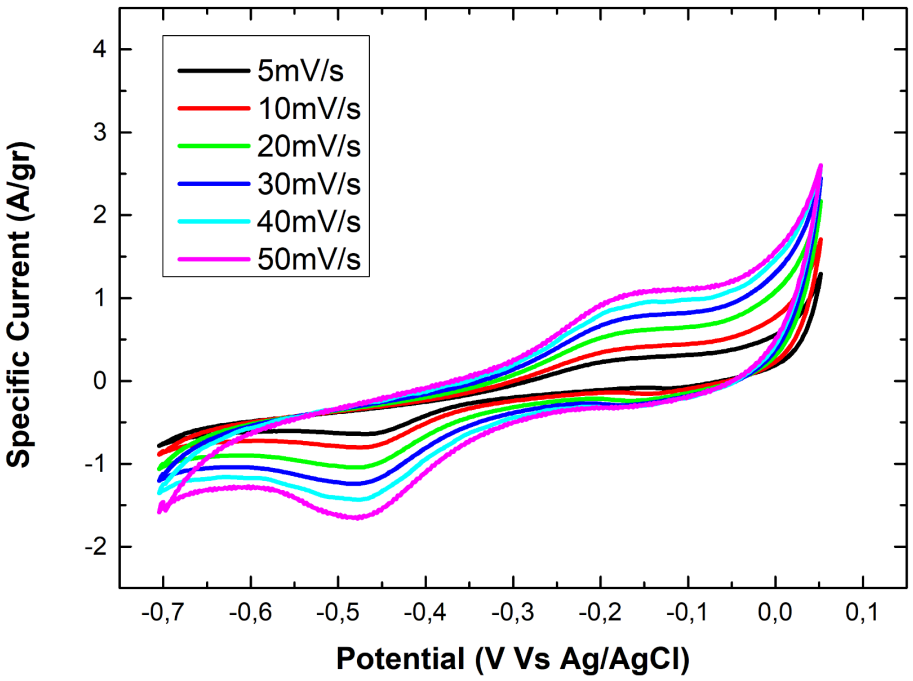


Figure 6.6 *Specific Current-Potential curves of electrodeposited GO for 0.25mA/cm² at different scan rates ranging from 5 to 50 mV/s.*

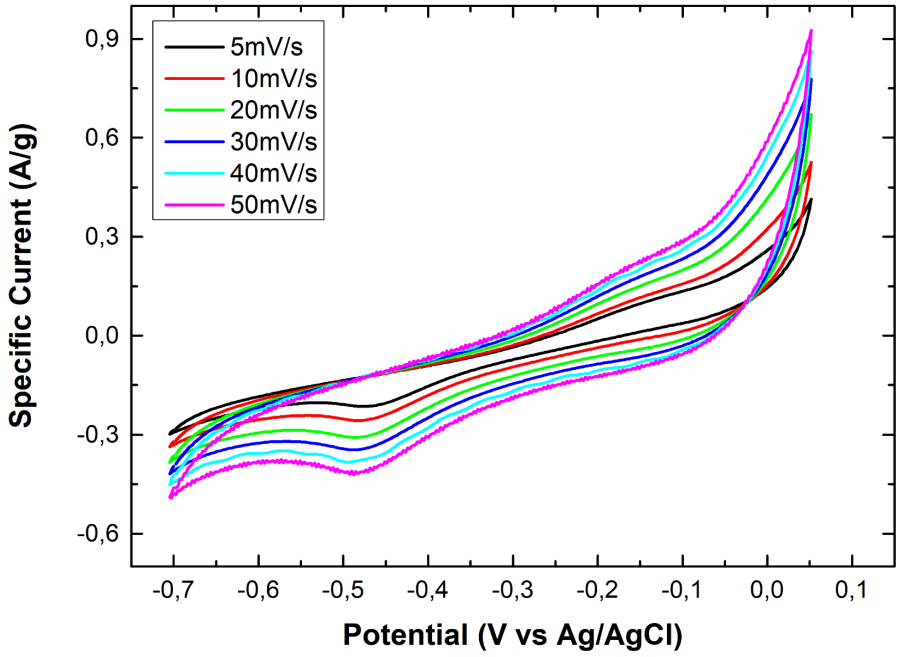


Figure 6.7 *Specific Current-Potential curves of electrodeposited GO for 0.5 mA/cm² at different scan rates ranging from 5 to 50 mV/s.*

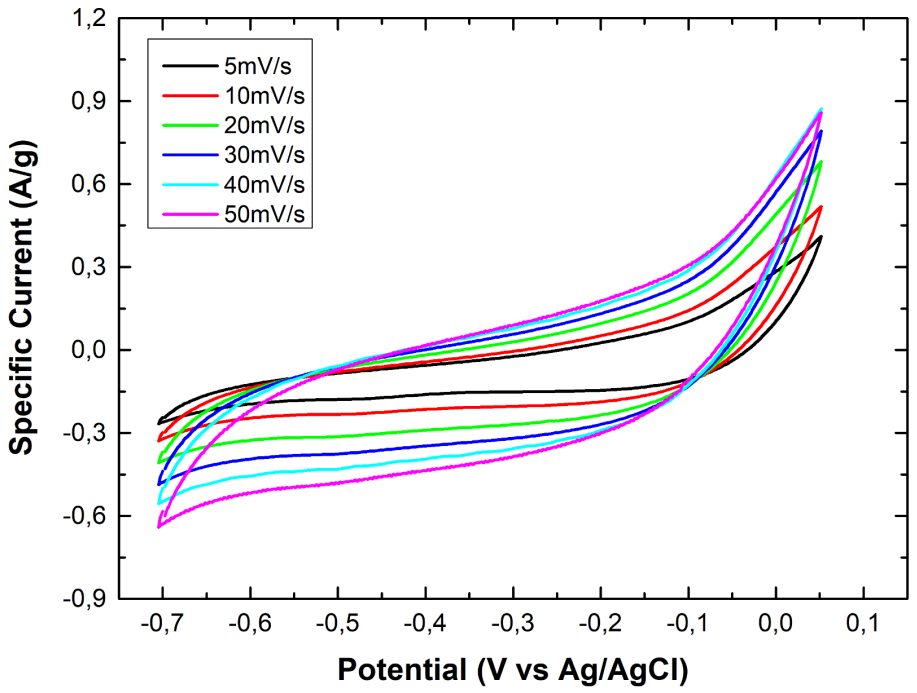


Figure 6.8 *Specific Current-Potential curves of electrodeposited GO for 0.75 mA/cm^2 at different scan rates ranging from 5 to 50 mV/s.*

Figures 6.6, 6.7 and 6.8 show the different scan rates of the three samples. As can be observed, the sample with the lowest deposition current density shows clear peaks compared to the other two samples, which have no peaks with the specific current much lower. This leads to the conclusion that the differences in electrochemical performance among the samples are related with their properties and they need to be investigated further.

According to the study accomplished in this Chapter, it is concluded that there was no relative improvement in the properties of the material (for example on the effective surface area) for higher deposition current density.

6.4 References

[1] López-Díaz D., Juan A. Delgado N., Clericò V., Diez E., Dolores Merchán M, and Mercedes Velázquez M., 2020. "Towards Understanding the Raman Spectrum of Graphene Oxide: The Effect of the Chemical Composition" Coatings 10, no. 6,524, https://doi.org/10.3390/coatings10060524

CHAPTER 7. Conclusions

The immobilization of GO, prepared by the Hummer method, was successfully carried out through the electrodeposition technique. The growth mechanism of the GO on Cu was thoroughly examined in relation to deposition conditions and electrolyte concentration. The structure and morphology of the GO were meticulously examined using Raman spectroscopy, SEM/EDS and XPS. Electrochemical analysis showed a subsequent increase in specific current over 600 intercalation/deintercalation cycles in specific current up to 2 A/gr in 600 intercalation/deintercalation cycles with 0.1 M Li_2SO_4 electrolyte with a diffusion coefficient $2.1x10^{-10}$ cm^2 s^{-1}. The sample demonstrated satisfactory stability at different electrolyte concentrations. In conclusion, one can conclude that graphene oxide could be a potential buffer layer for anode electrodes for energy storage device applications.

One potential area for future research could focus on exploring the growth mechanism of graphene oxide on various substrates, examining how different electrolytes and/or pH levels influence this process. Additionally, there's an opportunity to delve into synthesizing composites that incorporate GO with other carbon-based materials like activated carbon, carbon nanotubes, and biochar. This could help confirm the efficacy of such composites as buffer layers in the anodes and cathodes of lithium batteries.